Dissertation

Characterization of the molecular role of TRICA in oscillatory Ca^{2+} signaling

submitted by

Niroj SHRESTHA

for the Academic Degree of

Doctor of Philosophy (Ph.D.)

at the

Medical University of Graz

Gottfried Schatz Research Center

Department of Biophysics

under the Supervision of

Prof. Dr. Klaus Groschner

2019

Declaration

I hereby declare that this thesis is my own original work and that I have fully acknowledged by name all of those individuals and organizations that have contributed to the research for this thesis. Due acknowledgement has been made in the text to all other materials used. Throughout this thesis and in all related publications, I have followed the “Standards of Good Scientific Practice and Ombuds Committee at the Medical University of Graz”.

Graz, 20.05.2019

Niroj Shrestha

Disclosures

Part of this thesis has been published in:

1. Tiapko O*, **Shrestha N***, Lindinger S, Guedes de la Cruz G, Graziani A, Klec C, Butorac C, Graier WF, Kubista, Freichel M, Birnbaumer l, Romanin C, Glasnov T, Groschner K. 2019. Lipid-independent control of endothelial and neuronal TRPC3 channels by light. Chem Sci, 10(9), 2837-2842.
   *shared first authors (contributed equally)
2. Groschner K, **Shrestha N**, Fameli N. 2018. Non-Orai Partners of STIM Proteins: Role in ER-PM Communication and Ca^{2+} Signaling. In: Kozak JA, Putney JW, Jr., editors. Calcium Entry Channels in Non-Excitable Cells. Boca Raton (FL). 177-96.
3. Groschner K, **Shrestha N**, Fameli N. 2017. Cardiovascular and Hemostatic Disorders: SOCE in Cardiovascular Cells: Emerging Targets for Therapeutic Intervention. Adv Exp Med Biol, 993, 473-503.

All co-authors and their institutions who actively contributed to the results of the thesis and the publications resulting from the thesis project are listed below:

Klaus Groschner[1], Bernadett Bacsa[1], Oleksandra Tiapko[1], Annarita Graziani[1], Hwei Ling Ong[2], Indu Suresh Ambudkar[2], Christiane Klec[3], Roland Malli[3], Wolfgang. F. Graier[3], Sonja Lindinger[4], Carmen Butorac[4], Christoph Romanin[4], Gema Guedes de la Cruz[5], Toma Glasnov[5], Helmut Kubista[6], Marc Freichel[7], Lutz Birnbaumer[8,9]

[1]Gottfried Schatz Research Centre-Biophysics, Medical University of Graz, Graz, Austria
[2]Secretory Physiology Section, NIDCR, National Institutes of Health, Bethesda, MD, USA
[3]Gottfried Schatz Research Centre-Molecular Biology and Biochemistry, Medical University of Graz, Graz, Austria
[4]Institute of Biophysics, University of Linz, Linz, Austria
[5]Institute of Chemistry, University of Graz, Graz, Austria
[6]Institute of Pharmacology, Medical University of Vienna, Vienna, Austria
[7]Institute of Pharmacology, Heidelberg University, Heidelberg, Germany
[8]Neurobiology Laboratory, National Institute of Environmental Health Sciences, Research Triangle Park, North Carolina, USA
[9]Institute of Biomedical Research, Catholique University of Argentina, Buenos Aires, Argentina

I confirm that all co-authors have explicitly agreed to the use of their data in my thesis. I further confirm that I have obtained permission to reproduce the published figures and table and mentioned the details in the respective figures and table in the thesis.

Acknowledgement

I take this opportunity to thank my supervisor Prof. Klaus Groschner for giving me the opportunity to carry out the PhD dissertation in his lab. His continuous guidance and support throughout the project and materialization of the thesis is highly appreciated.

I am grateful to the Austrian Science Fund (FWF), Doctoral College in Metabolic and Cardiovascular Disease (DK-MCD) PhD program (grant number W1226), and Medical University of Graz for the financial support and for giving the opportunity to conduct part of my research at National Institutes of Health (NIH), Bethesda, USA.

I express my gratitude to my Ph.D. dissertation committee members, Roland Malli, and Simon Sedej, for their valuable support, discussion and suggestions during the project.

I consider myself fortunate to carry out my six-month abroad research in Indu Suresh Ambudkar's lab at NIH, Bethesda, USA. I convey my sincere thanks to her and Hwei Ling Ong for the scientific discussion, technical support, data analysis, and interpretation.

I would like to thank my lab colleagues Bernadett Bacsa, Michael Poteser, Rainer Schindl, Barbora Svobodova and Oleksandra Tiapko for the scientific discussion and technical support. I appreciate Sarah Krenn, Patrik Wiedner, Gebhard Schratter, Markus Waldeck-Weiermair, and Benjamin Gottschalk for the technical assistance. I am grateful to Hiroshi Takeshima and Christoph Romanin for sharing the plasmids.

I highly appreciate Chintan N. Koyani for always being there to discuss the data and troubleshoot the experiments. My hearty thanks to him and other friends for their personal and professional support. I would like to thank all the colleagues at the biophysics department for the friendly environment and off-work activities.

Last but not least, I heartily thank my family for all the support and encouragement throughout my Ph.D.

Niroj Shrestha

Table of contents

Abbreviations and Definitions

aa	amino acid
ATP	adenosine triphosphate
BHQ	2,5-Di-t-butyl-1,4-benzohydroquinone
BTP2	N-[4-[3,5-Bis(trifluoromethyl)pyrazol-1-yl]phenyl]-4-methylthiadiazole-5-carboxamide
$[Ca^{2+}]_{ER}$	ER luminal Ca^{2+} levels
$[Ca^{2+}]_i$	intracellular Ca^{2+} levels
$[Ca^{2+}]_o$	extracellular Ca^{2+} levels
CAD	CRAC activation domain
CaMKII	Ca^{2+}/calmodulin-dependent protein kinase II
cAMP	cyclic adenosine monophosphate
Ca_v channel	voltage-gated Ca^{2+} channel
CC	coiled-coil
CCh	carbachol
CFP	cyan fluorescent protein
CICR	Ca^{2+}-induced Ca^{2+} release
Co-IP	co-immunoprecipitation
CRAC channel	Ca^{2+} release-activated Ca^{2+} channel
DAG	diacylglycerol
EC coupling	excitation-contraction coupling
FRET	Förster resonance energy transfer
GPCR	G protein-coupled receptor
GST	glutathione S-transferase
HEK293	human embryonic kidney 293
I_{CRAC}	Ca^{2+} release-activated Ca^{2+} current
IP_3R	inositol 1,4,5-trisphosphate receptor
K_d	dissociation constant
NCX	Na^+/Ca^{2+} exchanger
NFAT	nuclear factor of activated T-cells
NMR	nuclear magnetic resonance
OASF	Orai-activating small fragment
PIP2	phosphatidylinositol-4,5-biphosphate
PLC	phospholipase C
PLN	phospholamban
POST	partner of STIM1
PKA	protein kinase A
PM	plasma membrane
PMCA	plasma membrane Ca^{2+}-ATPase

RyR	ryanodine receptor
SAM	sterile α-motif
SARAF	SOCE-associated regulatory factor
SCID	severe combined immunodeficiency
SERCA	sarco/endoplasmic reticulum Ca^{2+}-ATPase
SOAR	STIM–Orai activating region
SOCE	store-operated Ca^{2+} entry
SOICR	store-overload-induced Ca^{2+} release
SR/ER	sarco/endoplasmic reticulum
STIM	stromal interaction molecule
STIMATE	STIM-activating enhancer
TBST	Tris-buffered saline containing 0.1% Tween 20
TIRF	total internal reflection fluorescence
TM	transmembrane
TRIC channel	trimeric intracellular cation channel
TRPC channel	transient receptor potential canonical channel
VSMC	vascular smooth muscle cell
YFP	yellow fluorescent protein

List of Figures

List of Tables

Abstract in German

Trimere intrazelluläre Kationenkanäle (TRIC) sind an der Kontrolle der Ca^{2+} Freisetzung aus dem endoplasmatischen Retikulum (ER) beteiligt. Diese Ionenkanäle werden selbst durch den luminalen Ca^{2+} Spiegel im ER reguliert und ermöglichen einen Kationenstrom, welcher Ladungsausgleich und damit verstärkte Ca^{2+} Freisetzung aus dem ER ermöglicht ("counterion flux"). Die TRICA Isoform ist vorwiegend in erregbaren Geweben exprimiert und scheint damit insbesondere für zyklische, oszillierende Ca^{2+} Signale von Bedeutung. Die vorliegende Arbeit hatte das Ziel die zelluläre und molekulare Funktion von TRICA zu klären und präsentiert ein völlig neues mechanistisches Konzept der Frequenzmodulation von Ca^{2+} Signalen, das auf einer dynamischen Wechselwirkung zwischen TRICA und STIM/Orai Komplexen basiert. Unter Verwendung des HEK293 Exressionssystems konnten wir zeigen, dass TRICA Expression sowohl die Amplitude als auch die Frequenz von Ryanodin-Rezeptor (RyR2)-abhängigen Ca^{2+} Oszillationen aber auch Inositol trisphosphat (IP_3)-mediierte Ca^{2+} Signale durch Hemmung des Speicher-regulierten Ca^{2+} Einstroms (SOCE) unterdrückt. Dabei erscheint insbesondere der Ca^{2+} Rücktransport, also die Wiederauffüllung des ER Ca^{2+} Speichers, TRICA-abhängig verzögert und damit die Frequenz der zyklischen Signale verlangsamt. Bei ER-Ca^{2+} Entleerung translociert TRICA zusammen mit STIM1 in Regionen der Plamamembran („ER-PM junctions"), welche für SOCE verantwortliche Ionenkalkomplexe (STIM/Orai) enthalten. TRICA verzögert und hemmt die Ausbildung funktioneller STIM/Orai Kanalkomplexe und damit SOCE. Die vorliegende Arbeit identifiziert TRICA als einen neuen negativen Regulator der zellulären STIM/Orai Funktion und als ein Molekül mit potenzieller in pathophysiologischer Bedeutung speziell im Bereich von Muskelfunktionsstörungen.

Abstract in English

Trimeric intracellular cation (TRIC) channels reside in the sarco/endoplasmic reticulum (SR/ER) and have been proposed to sense luminal Ca^{2+} and modulate ER Ca^{2+} release by providing counterion flux. The TRICA isoform is expressed predominantly in the excitable tissues and appears to modulate the oscillatory Ca^{2+} signaling. This thesis is aimed at elucidating the molecular functions of TRICA and provides evidence for a novel concept of frequency modulation in oscillatory Ca^{2+} signaling, based on dynamic targeting of TRICA into STIM1/Orai1 complexes. Using a HEK293 reconstitution approach, we identified TRICA modulates the amplitude and frequency of RyR2-mediated Ca^{2+} oscillations and IP_3R-induced cytosolic signals by attenuating store-operated Ca^{2+} entry (SOCE). Further, TRICA-dependent delay in ER Ca^{2+} refilling contributes to shaping the pattern of Ca^{2+} oscillations. Upon ER Ca^{2+} depletion, TRICA co-migrates with STIM1, clusters with STIM1 and Orai1 within ER-plasma-membrane (PM) junctions, and impairs assembly of STIM1/Orai1 complex, causing a decrease in Orai1-mediated Ca^{2+} current and SOCE. Together, our findings demonstrate that TRIC-A is a negative regulator of STIM1/Orai1 function. Thus, upregulation of SOCE could contribute to muscle disorders associated with loss of TRICA.

Introduction

1.1 Trimeric intracellular cation (TRIC) channels

TRIC channels in vertebrates exist in two isoforms, TRICA and TRICB. TRICA was discovered in rabbit skeletal muscle as a 33k kDa protein while screening membrane proteins involved in intracellular Ca^{2+} handling, whereas its structural homolog, TRIC-B, was identified in homology searches in databases. While TRICB is ubiquitously expressed as an endoplasmic reticulum (ER)-resident channel in most mammalian tissues, TRICA is preferentially localized throughout the sarcoplasmic reticulum (SR) and nuclear membranes of excitable tissues, including skeletal muscles, heart, and brain (Yazawa et al., 2007). TRICA is predominantly expressed in skeletal muscles, compared to ryanodine receptor 1 (RyR1) and TRICB channels (5:1:1) (Zhao et al., 2010), whereas both TRIC isoforms have a similar expression in vascular smooth muscles (Yamazaki et al., 2011). Within the vertebrate family, TRICA shares 50-70% sequence identity, whereas TRICB shares about 40% sequence identity. The invertebrate TRIC homologs share about 30% sequence identity with either mammalian TRICA or TRICB (Wang et al., 2019).

1.1.1 Structure

Chemical cross-linking and electron microscopy using colloidal gold-conjugated Fab fragments labeling of TRICA purified from skeletal muscle microsomes demonstrated a homotrimeric pyramidal structure (Yazawa et al., 2007). Later, crystal structures of non-mammalian TRIC homologs from X-ray crystallography revealed homotrimeric complexes, stabilized by lipids. Each monomer consists of an hourglass-shaped, hydrophilic pore within seven transmembrane helices (TM1–7) with a luminal N-terminus and a cytosolic C-terminus (Figure 1). The electrostatic potential is slightly negative on the luminal side and largely positive on the cytosolic side (Yang et al., 2016, Wang et al., 2019).

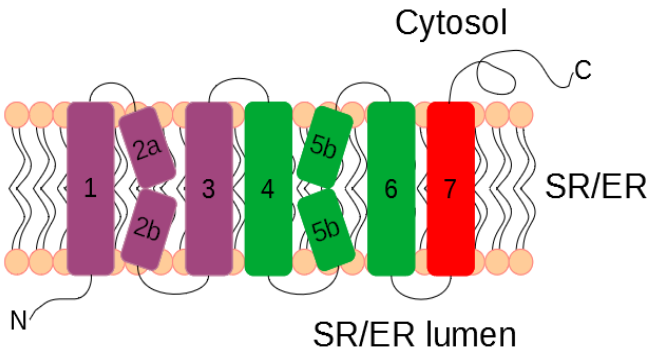

Figure 1. Membrane topology of TRIC channel monomer.

Each monomer consists of seven transmembrane helices (TM1–7) where TM4-6 (green) resemble the inverted repeats of TM1-3 (purple) attached to luminal N-terminus, and TM7 (red) exists as standalone helix attached to cytosolic C-terminus.

TM5b acts as a conformational switch for binding different lipid molecules at the monomer interfaces like phosphatidylinositol-4,5-bisphosphate (PIP2) in invertebrates like *Caenorhabditis elegans* or diacylglycerol (DAG) in vertebrates (Figure 2). While these lipids have been reported to activate ion-channels like transient receptor potential canonical (TRPC), Kir channels on the PM, they stabilize the homotrimeric complex of TRIC channels (Tiapko et al., 2019, Yang et al., 2016, Wang et al., 2019). The polar head of lipids orients towards the monomeric pore whereas the non-polar acyl chains face towards the trimeric center (Yang et al., 2016, Wang et al., 2019).

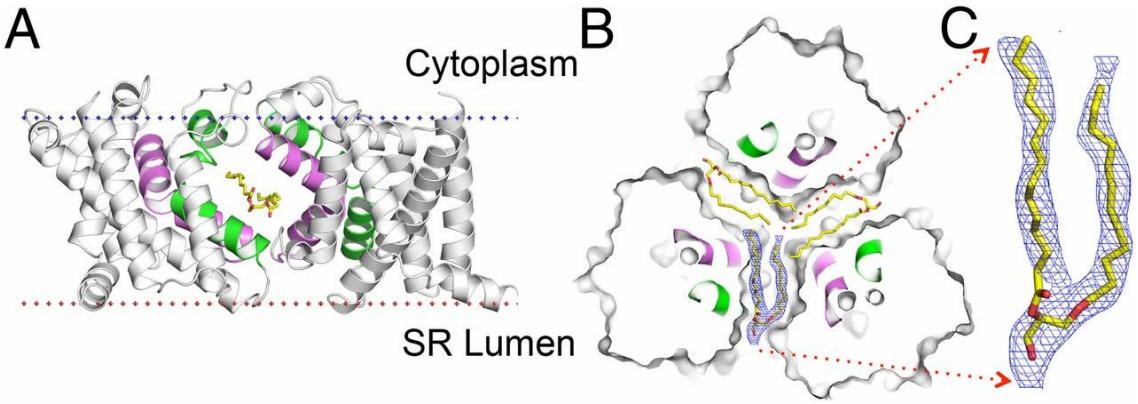

Figure 2. TRICA complex with lipid.

(A) Ribbon diagram of *Gallus. gallus* TRICA, with one monomer removed. The TM2 (purple) and TM5 (green) helices from two monomers line the lateral fenestration in which the lipid molecules (DAG) are shown as sticks, with carbon (yellow), nitrogen (blue), and oxygen (red). **(B)** Cross-section view of *G. gallus* TRICA with three DAG molecules superimposed into the lateral fenestrations. **(C)** Enlarged view of the DAG molecule, shown in B. *Reproduced from (Wang et al., 2019) with permission from PNAS.*

At rest, cation permeation in *Gallus gallus* TRICA appears occluded by a highly conserved Lys^{129} residue within a voltage-sensing region in TM4 (KEVXRXXK), which forms hydrogen bonds with Tyr^{29} (TM1) and Ser^{65} (TM2). The pore blockage is stabilized by Ca^{2+} binding to the highly conserved Gly^{74} at the luminal channel surface, together with the hydrogen bonds among the polar residues of TM helices. The conserved basic residues that line the pore and the voltage-sensing region is balanced by the phosphate groups of lipids and the acidic residues (Figure 3, left). Dissociation of Ca^{2+} from TRICA was shown to initiate a conformational transition, accompanied by the loss of nearly all stabilizing hydrogen bonds (Figure 3, right) which is expected to move the Lys^{129} plug and open the pore for counterion flux in a voltage-dependent manner (Wang et al., 2019).

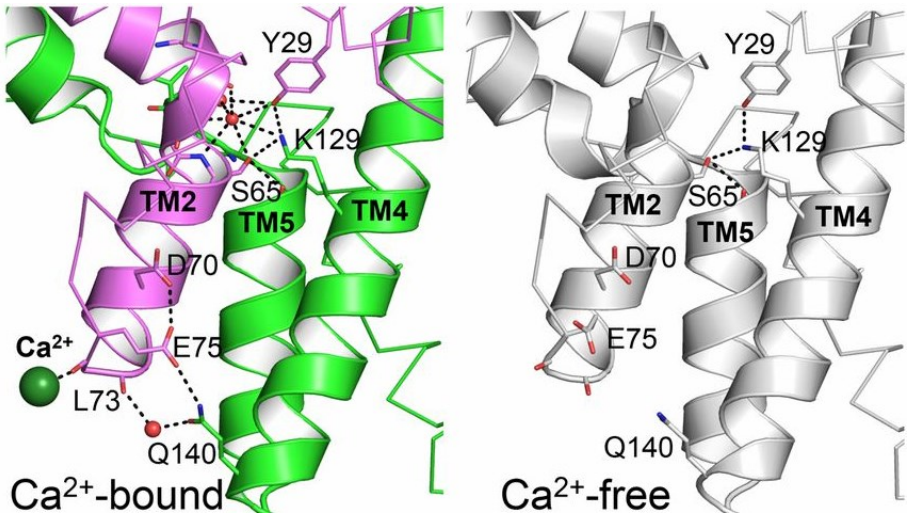

Figure 3. Ca^{2+} binding and modulation in TRIC channels.
Membrane view of Ca^{2+}-bound (left, dark green sphere) and Ca^{2+}-free structures of *G. gallus* TRIC-A along with water molecules (red sphere). The amino residues (sticks) are involved in hydrogen bonding (black dashed lines). *Reproduced from (Wang et al., 2019) with permission from PNAS.*

1.1.2 Ion-Permeability

The single channel properties (conductance and gating) of purified/recombinant TRIC isoforms have been studied extensively in lipid bilayer reconstitution experiments. TRICA purified from rabbit skeletal SR vesicles is permeable to monovalent cations, K^+ over Na^+ (permeability ratio=1.5) with a reversal potential of -20 ± 1.7 mV but impermeable to divalent cations and anions (Yazawa et al., 2007).

1.1.3 Regulatory factors

1.1.3.1 Voltage

TRIC channels, mainly TRICA, are regulated by trans-SR voltage with higher open probability, mean dwell time and current amplitude at positive holding potentials on the cytosolic side relative to the SR lumen (Pitt et al., 2010, Wang et al., 2019). The TRICA channel pore mutant K129A is constitutively active at all voltages whereas K129Q mutant is largely closed, indicating a significant role of the highly conserved Lys^{129} residue in gating as well as sensing voltage across the sarco/endoplasmic reticulum (SR/ER) (Wang et al., 2019).

Out of two conductance states, TRICA gate predominantly to a fully open state, with a brief, occasional transition to subconductance state (Pitt et al., 2010). On the other hand, TRICB have multiple subconductance states in addition to a fully open state (Pitt et al., 2010, Venturi et al., 2013). Besides, three monomers in the homotrimeric homolog in *C. elegans* were found to function cooperatively to achieve rapid, simultaneous opening of all pores for the cation permeation (Yang et al., 2016).

1.1.3.2 Luminal and cytosolic Ca^{2+}

TRIC channels act as Ca^{2+} sensors in both SR/ER lumen and cytosol. Single-channel current of TRICB is inhibited by luminal Ca^{2+} and activated by micromolar cytosolic Ca^{2+} (Pitt et al., 2010). TM5-6 loop in TRICB homolog is proposed as a Ca^{2+} sensing domain on the cytosolic side, which undergoes a conformational change upon Ca^{2+} binding and favors voltage-dependent channel opening for monovalent cation permeation (Yang et al., 2016). Besides, luminal Ca^{2+} (0.5-1.0 mM) inhibits voltage-activated single channel current of purified *G. gallus* TRICA, possibly due to substantial pore stabilization by bound Ca^{2+} (Wang et al., 2019).

1.1.4 (Patho)physiological role in Ca^{2+} signaling

Ca^{2+} is a universal second messenger that regulates a plethora of cellular functions, including excitation-contraction (EC) coupling, secretion, gene expression, differentiation and apoptosis. Distinct Ca^{2+}-selective channels and transporters localized in various cellular compartments at varying levels in different

cell types confer cell-type specific Ca^{2+} signals with spatial and temporal precision (Berridge et al., 2000).

Ca^{2+} signals are initiated by a rise in cytosolic Ca^{2+} level via release from intracellular SR/ER stores or influx across the plasma membrane (PM) from the extracellular space. SR/ER Ca^{2+} is released through two distinct families of ion channels: RyRs and inositol 1,4,5-trisphosphate receptors (IP_3Rs) (Berridge et al., 2000). IP_3Rs are ubiquitously expressed and are activated by IP_3 and low (<1 μM) local, cytosolic Ca^{2+} but inhibited at higher cytosolic Ca^{2+} (1-10 μM). IP_3 is formed from hydrolysis of PIP2 by activated phospholipase C (PLC), following stimulation of specific cell surface receptors. RyRs are the largest known ion channels and exist in 3 isoforms (RyR1-3), mainly in excitable tissues such as skeletal muscles, cardiac muscles, and neurons respectively. RyRs are mainly regulated via its large cytosolic region by various modulators namely Ca^{2+} and Mg^{2+} ions, voltage-gated Ca^{2+} (Ca_v) channel, calmodulin, adenosine triphosphate (ATP), FK506 binding proteins (FKBP12 and 12.6), protein kinase A (PKA), Ca^{2+}/calmodulin-dependent protein kinase II (CaMKII), calsequestrin, triadin, and junctin. RyRs are activated at 1-10 μM and inhibited at 10-100 μM cytosolic Ca^{2+}.

The elevated cytosolic Ca^{2+} following release from SR/ER is mainly pumped back by sarco/endoplasmic reticulum Ca^{2+}-ATPase (SERCA) or extruded out of the cell by plasma membrane Ca^{2+}-ATPase (PMCA) or Na^+/Ca^{2+} exchanger (NCX). Mitochondria also play a role in buffering cytosolic Ca^{2+} through their low affinity but high capacity Ca^{2+} uniporter (Berridge et al., 2000). Ca^{2+} efflux from SR/ER lumen to the cytosol through the RyR and/or IP_3R gives rise to a transient negative potential within the SR/ER lumen (Figure 4). TRIC channels have been postulated to provide counter monovalent cation flux (mainly K^+) to neutralize the negative potential and facilitate further Ca^{2+} release (Yazawa et al., 2007).

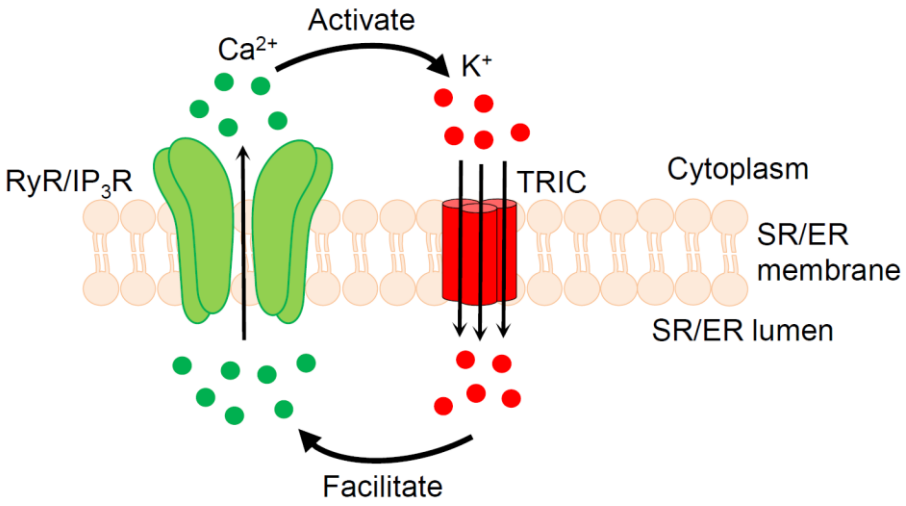

Figure 4. Schematic illustration of the proposed role of TRIC channels during SR/ER Ca^{2+} release.

TRIC channels provide counter monovalent cation flux (mainly K^+) to neutralize the transient negative potential generated SR/ER Ca^{2+} release via RyR/IP_3R and facilitate further Ca^{2+} release.

Gene knockout studies demonstrate that TRIC channels are essential for the normal physiology of various tissues and even survival. Mice with a knockout of both subtypes die of heart failure before birth where embryonic cardiomyocytes display weak spontaneous RyR-mediated Ca^{2+} oscillations but enhanced caffeine-evoked Ca^{2+} transients, due to Ca^{2+} overload in swollen, abnormal SR (Yazawa et al., 2007). TRICB knockout mice die immediately after birth due to respiratory failure, characterized with compromised IP_3R-mediated Ca^{2+} release and ultrastructural abnormalities in alveolar epithelial cells (Yamazaki et al., 2009). On the other hand, TRICA knockout mice are viable with normal growth, reproduction and motor functions but exhibit abnormal SR Ca^{2+} mobilization in excitable muscles (Yazawa et al., 2007, Zhao et al., 2010, Yamazaki et al., 2011).

Isolated skeletal muscle fibers from TRICA knockout mice exhibit more negative SR membrane potential, compromised osmotic stress-induced Ca^{2+} sparks and slower voltage-induced Ca^{2+} release via RyR1 (Yazawa et al., 2007). Further, they display higher Ca^{2+} release from caffeine-sensitive SR stores and irregular contractile force (mechanical alternans) during fatigue (Zhao et al., 2010). In addition, RyR1 gating is compromised in TRICA knockout mice where ATP (in the presence of Mg^{2+}), as well as PKA-dependent phosphorylation, failed to

effectively activate RyR1 though sensitivity to cytosolic or luminal Ca^{2+} and ATP remained unchanged (El-Ajouz et al., 2017).

In vascular smooth muscle cells (VSMCs), TRICA ablation inhibits RyR-mediated Ca^{2+} sparks under depolarizing conditions (high extracellular K^+) but enhances IP_3R-mediated Ca^{2+} waves and oscillations due to Ca^{2+} overload in IP_3-sensitive stores. Besides, VSMCs lacking TRICA has depolarized resting membrane potential due to less active Ca^{2+}-dependent K^+ channels. This, in turn, activates L-type Ca^{2+} channels to elevate cytosolic Ca^{2+} and resting tonus of VSMCs, leading to hypertension and bradycardia in TRICA knockout mice during the daytime, which is rescued via VSMC-specific TRICA transgene expression (Yamazaki et al., 2011). On the other hand, wild-type mice overexpressing TRICA in VSMCs develop hypotension owing to opposite effects on RyR and IP_3R (Tao et al., 2013).

The phenotypes observed as a consequence of TRICA knockout in muscle tissues were attributed to the lack of critical K^+ countercurrent via the trimeric channel during SR Ca^{2+} release. However, replacing cytosolic K^+ with Na^+ or Cs^+ in isolated cardiac SR microsomes or saponin-permeabilized myocytes markedly reduced the SR K+ channel conduction, yet failed to affect single RyR2 channel currents and open probability, as well as Ca^{2+} sparks and SR Ca^{2+} load. Moreover, RyRs have been proposed to provide themselves sufficient counter K^+/Mg^{2+} flux to enable and sustain Ca^{2+} release. Hence the TRIC channels may not represent an indispensable prerequisite for efficient SR Ca^{2+} release as presumed earlier, but still contribute to K^+ equilibrium across SR and in turn restore ER membrane potential near 0 mV upon closure of RyRs during repetitive cycles of release events (Guo et al., 2013). Recently, a cardiac SR compartment model simulation suggested that SR Ca^{2+} release relies on a cascading network of ion permeabilities including TRICs to provide countercurrents and establish ion homeostasis (Zsolnay et al., 2018).

1.2 Store-operated Ca^{2+} entry (SOCE)

1.2.1 Concept and history

Although SOCE has a long history in terms of a physiological phenomenon, it has been explored at the molecular ion-channel function only within the past 15 years. PLC-coupled agonists release Ca^{2+} from IP_3-sensitive intracellular stores and activate Ca^{2+} influx across the PM from extracellular space. The incoming Ca^{2+} is quickly diffused into ER, closely associated with PM, for privileged refilling of depleted stores. This concept of "capacitative Ca^{2+} entry" was first envisioned and proposed by Putney in 1986, based on previously published findings (Putney, 1986). In later experiments in parotid acinar cells, the Ca^{2+} influx was evident following depletion of intracellular stores not only by PLC-IP_3 pathway but also by inhibition of SERCA (Takemura and Putney, 1989). Thus, Putney revised his previous concept stating that Ca^{2+} influx via PM channels depends on the filling state within the intracellular Ca^{2+} stores, and can be activated by simply depleting the stores irrespective of the stimulus, now termed as store-operated Ca^{2+} entry (SOCE) (Putney, 1990). Hoth and Penner recorded whole-cell Ca^{2+} release-activated Ca^{2+} (CRAC) current, I_{CRAC} through PM channels, activated slowly following Ca^{2+} store depletion in the mast cells. I_{CRAC} is a highly Ca^{2+}-selective, non-voltage-gated, and inward rectifying current with positive reversal potential (Hoth and Penner, 1992). I_{CRAC} is small (few pA/pF) and the estimated single-channel conductance (<1 pS) is too low to be detected by conventional electrophysiology (Zweifach and Lewis, 1993).

Almost two decades after the conceptualization of the "capacitative Ca^{2+} entry" model, the molecular key players involved were identified via genome-wide RNA interference screens and genetic linkage analysis in patients. Stromal interaction molecules (STIM1 and STIM2) were identified as sensors for the ER luminal Ca^{2+} levels ($[Ca^{2+}]_{ER}$) (Roos et al., 2005, Liou et al., 2005) whereas Orai1 (also termed CRACM) was discovered as the essential component of CRAC channels at the PM (Feske et al., 2006, Vig et al., 2006b, Zhang et al., 2006). Following the molecular identification of STIM and Orai proteins, a number of structural, functional and biochemical studies have been carried out to compare the homologs, determine their stoichiometry, identify structural domains involved in clustering and interaction, and understand their (patho)physiological significance.

1.2.2 STIM

Although initially identified as a stromal cell surface molecule, which recognizes B-cell precursors and affects their proliferation (Oritani and Kincade, 1996), the role of STIM1 and its vertebrate homolog, STIM2 (Williams et al., 2001) in Ca^{2+} signaling was deciphered a decade later via function-based RNA interference screens (Roos et al., 2005, Liou et al., 2005). STIM proteins are predominantly and ubiquitously expressed in the ER membrane of various cells, and largely conserved across species. As shown in figure 5, they have single-TM domain, with EF-hand and sterile α-motif (SAM) at the luminal N-terminus, and coiled-coil domains (CC1 (α1-3), CC2 and CC3), inhibitory domain, Ser-/Pro-rich domain, and Lys-rich polybasic tail at the cytosolic C-terminus (Soboloff et al., 2012). The coiled-coil and Ser/Pro-rich domains mediate the comet-like movement of STIM1 along the microtubules via binding to EB1 (a microtubule-plus-end-tracking protein involved in microtubule-ER extension) (Baba et al., 2006, Grigoriev et al., 2008). STIM1 is a phosphoprotein, with phosphorylation sites between the inhibitory domain and polybasic tail (Pozo-Guisado et al., 2010). Apart from sensing $[Ca^{2+}]_{ER}$, STIM1 is triggered by various other stimuli, including oxidative stress, temperature, hypoxia, and acidification (Soboloff et al., 2011).

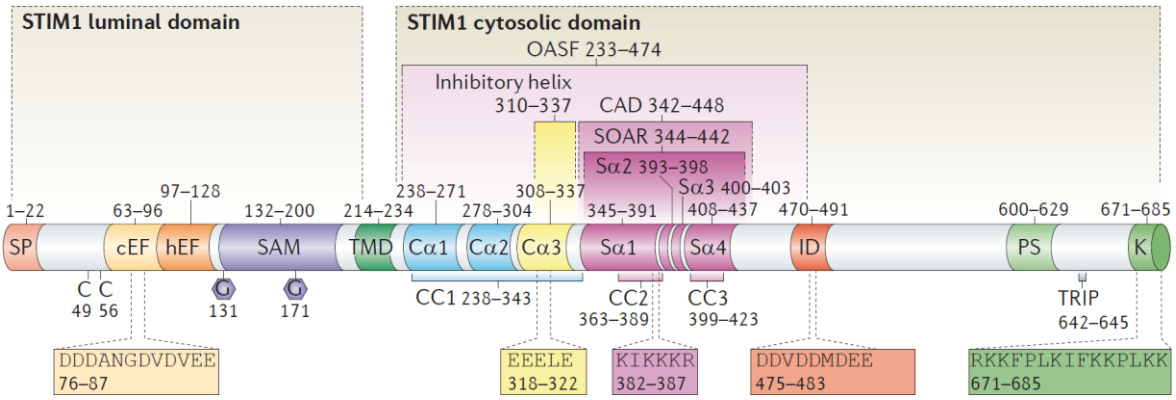

Figure 5. Molecular domains of human STIM1.

SP, signal peptide (SP); cEF, Ca^{2+}-binding canonical EF-hand; hEF, non-Ca^{2+}-binding hidden EF-hand; SAM, sterile α-motif; TMD, transmembrane domain; CC1 (Cα1, Cα2 and Cα3), CC2 and CC3, coiled-coil regions; SOAR, STIM–Orai activating region; CAD, Ca^{2+} release-activated Ca^{2+} (CRAC) activation domain; OASF, Orai-activating small fragment; Sα1, Sα2, Sα3 and Sα4, four α-helices; ID, inhibitory domain; PS, Pro/Ser-rich domain; TRIP, microtubule interacting domain; K, polybasic domain. *Reproduced from (Soboloff et al., 2012) with permission from Springer Nature (Order number: 4575880927132).*

At resting $[Ca^{2+}]_{ER}$ of ~400 μM (Figure 6), STIM1 exits as an inactive, folded dimer, stabilized by intramolecular interactions within Orai-activating small fragment (OASF, aa 233-474) composed of CC1 (aa238-343) and STIM-Orai activating region (SOAR, aa344-442) or CRAC activation domain (CAD, aa342-448) in the cytosolic region (Yuan et al., 2009, Covington et al., 2010, Muik et al., 2011). Two studies provided structural insights into the cytosolic CC domains of STIM1 (Yang et al., 2012, Stathopulos et al., 2013). First, a crystal structure of V-shaped human SOAR dimer revealed that each R-shaped SOAR consists of four α-helices (Sα1-Sα4, aa 345-444) in which Sα1 (CC2) of one SOAR interacts with Sα4 (CC3) of another SOAR. These dimeric interactions are critical for further coupling to and activation of Orai1 (Yang et al., 2012). In addition, the crystal structure of CC1 and SOAR fragments of *C. elegens* STIM indicated that the acidic residues (aa318-322) within CC1α3 helix (aa310-337) interacts with the two ends of SOAR (CC2 and CC3) to restrict cytosolic region of STIM1 in an inactive, folded conformation (Yang et al., 2012). Second, a solution nuclear magnetic resonance (NMR) structure of human STIM1 aa312–387 revealed that CC1α3 and CC2 bend in between to form dimers in an antiparallel manner.

Various mutation analyses have confirmed the critical role of CC1-CC3 interaction in restricting STIM1 in an inactive, folded conformation. Mutations in the CC1α3 inhibitory helix disrupt the electrostatic and hydrophobic interactions, and coiled conformation, unfold SOAR into active, extended conformation (Korzeniowski et al., 2010, Muik et al., 2011, Yu et al., 2013) whereas disrupting the amphipathic property of CC1α3 inhibitory helix locks STIM1 in a closed conformation, unable to respond to store depletion (Yu et al., 2013). Furthermore, mutation(s) within CC1α1 helix releases STIM1 into an extended, constitutively active state (Muik et al., 2011, Zhou et al., 2013, Fahrner et al., 2014). In contrast, CC1α2 seems to have a destabilizing role since CC1α1-CC3 interaction is stronger following CC1α2 deletion (Fahrner et al., 2014).

Two TM domains in the STIM1 dimer cross each other at an angle to separate the EF-SAM domains at the luminal region as monomers (Ma et al., 2015). The EF-hand of STIM1 is tightly associated with the SAM domain at the N-termini, which auto-inhibits oligomerization (Zheng et al., 2011). The negatively charged Glu and Asp residues of EF-hand are bound to luminal Ca^{2+} with a dissociation constant (K_d) of ~200 μM (Stathopulos et al., 2006). STIM2 has lower

Ca^{2+} affinity (K_d~400 μM) than STIM1 due to the substitution of three amino acids in the EF-hand and is more sensitive to small changes in $[Ca^{2+}]_{ER}$ (Brandman et al., 2007). Despite higher sensitivity to $[Ca^{2+}]_{ER}$, EF-SAM domain of STIM2 is stabilized by additional short, flexible N-terminal coiled residues, thereby preventing constitutive activation of Orai1 channels (Stathopulos et al., 2009, Zhou et al., 2009).

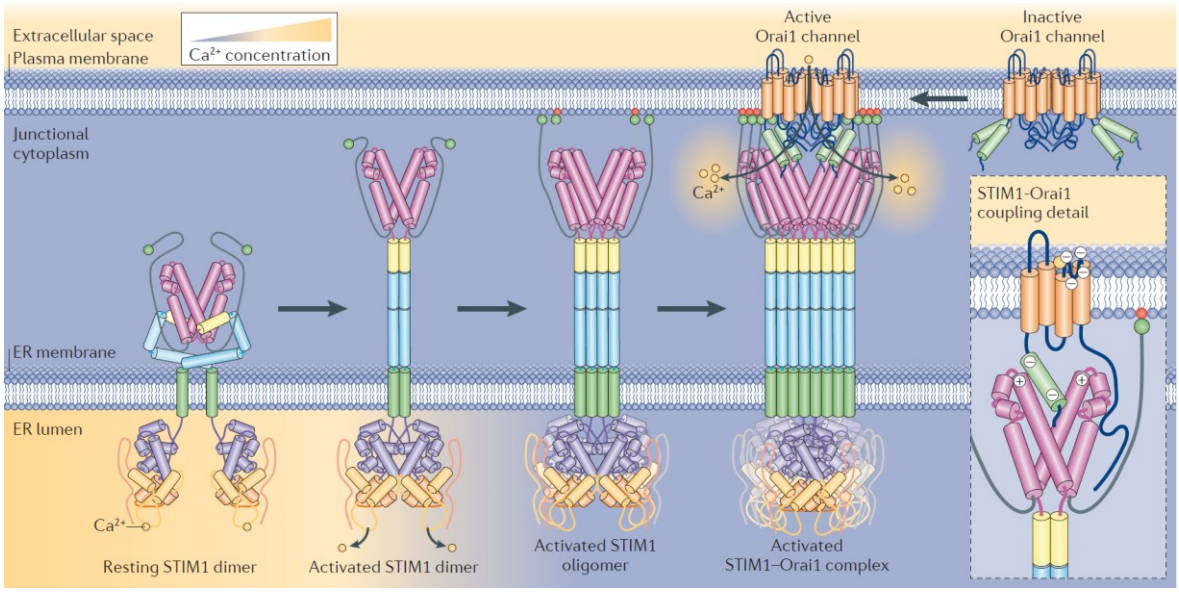

Figure 6. Graphical representation of STIM1 activation and coupling within ER-PM junctions. At rest, STIM1 is localized in the ER membrane as a dimer and bound to luminal Ca^{2+} via EF-hand. The molecular domains are coloured same as Figure 5. Dissociation of Ca^{2+} following ER Ca^{2+} depletion induces conformational changes where EF-SAM dimerizes and cytosolic coiled-coil domains unfold to extended configuration to expose SOAR. Activated STIM1 then oligomerizes and translocates into ER-PM junctions, and the polybasic C-termini anchor STIM1 to acidic phospholipids in the PM. STIM1 oligomers recruit, bind and activate Orai1 channels. *Reproduced from (Soboloff et al., 2012) with permission from Springer Nature (Order number: 4575880927132).*

Upon ER Ca^{2+} depletion (Figure 6), loss of bound Ca^{2+} destabilizes and unfolds EF-SAM complex to trigger oligomerization and translocation into discrete puncta at junctional ER, located within 25 nm from the PM, known as ER-PM junctions (Wu et al., 2006, Liou et al., 2007, Stathopulos et al., 2008). These junctions cover ~5% of PM surface at rest and can expand upon STIM activation (Wu et al., 2006). Mutations in EF-hand lowers its Ca^{2+} affinity so that STIM1 pre-clusters within ER-PM junctions without store depletion, leading to constitutive CRAC channel activation and Ca^{2+} influx (Liou et al., 2005, Zhang et al., 2005).

The EF-SAM oligomerization triggers change in the crossing angle of TM domains via conformational changes in three flexible glycine residues (Gly^{223}, Gly^{225}, and Gly^{226}), thereby propagating the activation signal throughout the cytosolic domain (Ma et al., 2016). The CC1 domain is then dissociated from SOAR/CAD (Korzeniowski et al., 2010, Muik et al., 2011, Yang et al., 2012, Yu et al., 2013, Zhou et al., 2013, Fahrner et al., 2014) so that CC1 homomerizes and SOAR unfolds to an extended conformation with strong interaction between CC2-CC3 domains within SOAR, which stabilizes the unstable EF-SAM oligomers of STIM1 (Yuan et al., 2009, Covington et al., 2010). STIM2 has more stable EF-SAM domain, resulting in slower unfolding and oligomerization upon Ca^{2+} dissociation (Stathopulos et al., 2009, Zheng et al., 2011), and in turn poor coupling to and slow activation of Orai1 (Zhou et al., 2009). Overexpressed STIM2, therefore, inhibits the rate and magnitude of endogenous STIM1-mediated SOCE (Soboloff et al., 2006a, Brandman et al., 2007).

1.2.3 Orai1

Humans encode three homologs (Orai1, Orai2, Orai3), conserved in the predicted four-TM helices with cytosolic N- and C-termini, and acidic residues involved in Ca^{2+}-binding and selectivity (Figure 7) (Prakriya and Lewis, 2015). Three independent RNA interference screens in *Drosophila* S2 cells identified *Drosophila* Orai (*olf186-F*) or its human homolog Orai1 as a key player in CRAC channel complex, involved in SOCE and downstream signaling of nuclear factor of activated T-cells (NFAT) (Feske et al., 2006, Zhang et al., 2006, Vig et al., 2006b). Of note, Orai1 was found to be mutated at a highly conserved Arg^{91} residue (R91W) in two homozygous patients suffering from severe combined immunodeficiency (SCID), leading to impaired I_{CRAC}, SOCE, and NFAT-dependent gene activation. Reconstitution of wild-type Orai1 in SCID T-cells restored I_{CRAC} and SOCE, establishing a critical role of Orai1 in T-cell function and immune response (Feske et al., 2006). Following store depletion, STIM1 interacts with and recruits Orai1 into discrete clusters within ER-PM junctions and activates Orai1 channels for Ca^{2+} influx (Luik et al., 2006). Orai1 expressed alone, reduces I_{CRAC} and SOCE, likely reflecting a required stoichiometry between STIM1 and Orai1 (Soboloff et al., 2006b).

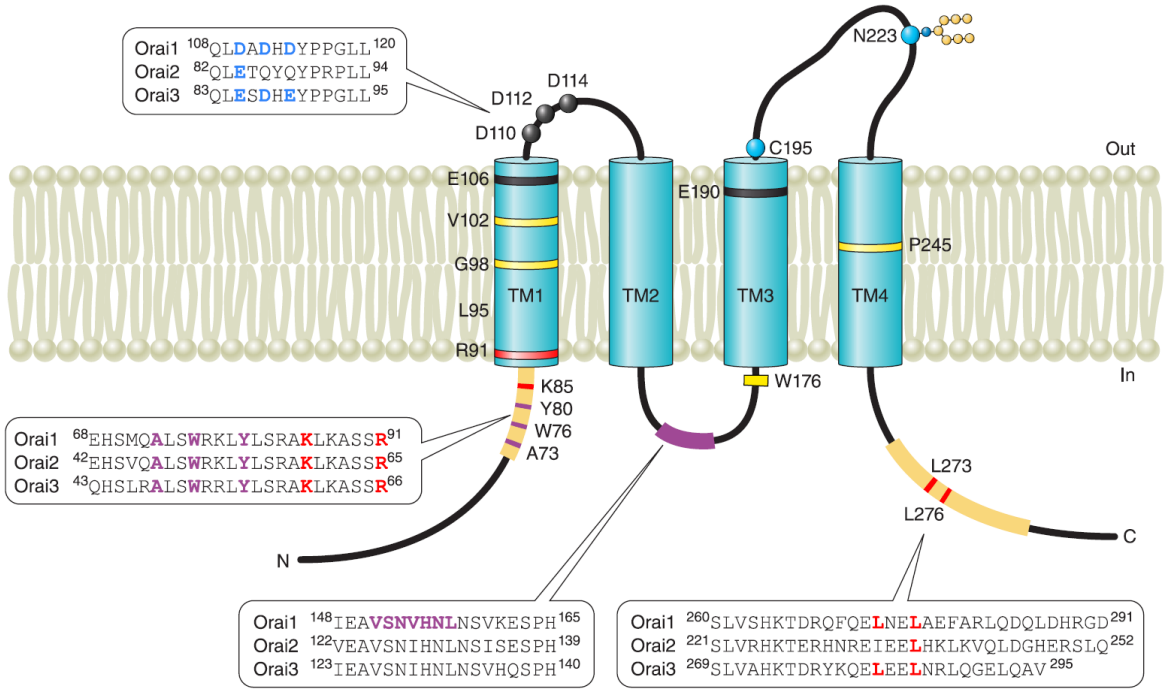

Figure 7. Membrane topology of Orai1 channel monomer.

Insets show a comparison of Orai1-3 protein sequences in N- and C-termini, and TM1-TM2 and TM2-TM3 loops. Yellow and red lines in TM, residues with gain-of-function and loss-of-function mutations respectively; black lines in TM, residues affecting ion-selectivity; red lines in N- and C-termini, residues important for STIM binding and gating; purple bars, intracellular residues critical for Ca^{2+}-dependent inactivation; black circles in TM1–TM2 loop, acidic residues; blue circles in TM3-TM4 loop, redox inhibition site (C195) and glycosylation site (N223). *Reproduced from (Prakriya and Lewis, 2015) with permission from The American Physiological Society (Order number: 4587650420763).*

Subsequently, the crystal structures of *Drosophila melanogaster* Orai in a closed form (Hou et al., 2012) and later in a constitutively open form (Hou et al., 2018) supported the findings from functional and biochemical studies and established Orai as the ion-selective pore of CRAC channel (Figure 8). First, a ring formed by conserved Glu^{178} residues (Glu^{106} in human Orai1) around the extracellular surface is critical for Ca^{2+} binding, selectivity, and permeability. Mutations at the Glu^{106} (E106A or E106Q) remove its negative charge in TM1 and block I_{CRAC}, whereas E106D reduces Ca^{2+} affinity and selectivity. Besides, mutating E190Q in TM3 facing the pore also reduces Ca^{2+} selectivity (Prakriya et al., 2006, Vig et al., 2006a). Close to the Glu^{106} selectivity filter, the acidic residues on the external loop between TM1 and TM2 form Ca^{2+} accumulation region, which increases local extracellular Ca^{2+} concentration and drives Ca^{2+} influx through the

pore (Frischauf et al., 2015). Second, the non-polar residues Leu^{167}, Phe^{171}, and Val^{174} (Leu^{95}, Phe^{99}, and Val^{102} in human Orai1) in TM1 helices line the narrow, rigid middle portion of the pore (McNally et al., 2009, Zhou et al., 2010b) which act as a barrier to ion flux in a closed state but move away during STIM1-dependent gating and rotation of pore helix to allow Ca^{2+} influx (Gudlur et al., 2014, Yamashita et al., 2017). Besides, V102A/V102C mutation transforms the channels into constitutively active and less selective, but the Ca^{2+}-selectivity can be restored by gating via co-expressed STIM1 (McNally et al., 2012, Yamashita et al., 2017). Third, basic residues Arg^{155}, Lys^{159}, and Lys^{163} (Arg^{83}, Lys^{87}, and Arg^{91} in human Orai1) in TM1 helices line the intracellular surface of the conductance pathway. R91W mutation was initially identified in SCID patients (Feske et al., 2006), where the bulky hydrophobic tryptophan rings could occlude the pore, resulting in compromised I_{CRAC}. Fourth, M4-ext helices facing cytosol stabilizes the interaction between M4b and M3 helices to constrain the pore in a closed conformation. When the M4-ext helices move away and interact with cytosolic regions of active, extended STIM1, the pore widens and opens for Ca^{2+} influx (Hou et al., 2018).

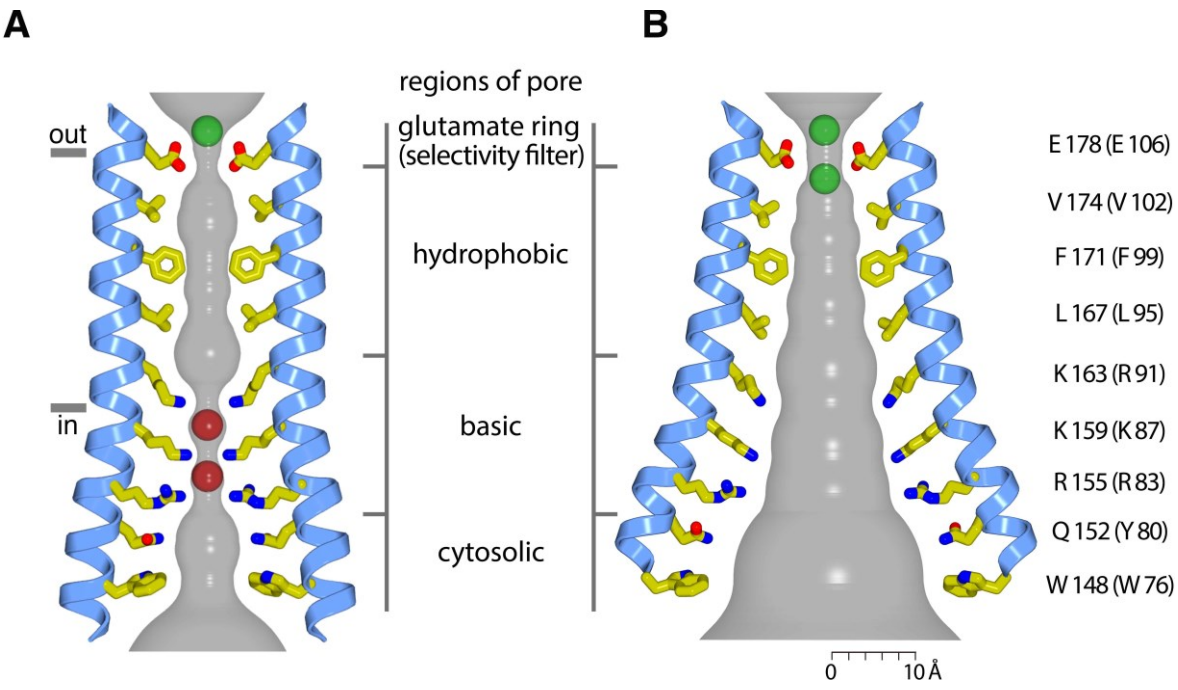

Figure 8. Ion conduction pores in (A) closed and (B) open conformation from *D. melanogaster* Orai crystal structures.

The pores are lined by amino acids (yellow) from two TM1 helices. The corresponding amino acids in human Orai1 are shown in parentheses. The gray surface represents the radial distance from the center to the nearest van der Waals protein contact. The horizontal lines depict approximate

boundaries of the membrane-spanning region. The sections of the pore discussed in the text are labeled. Green sphere, Ca^{2+}; red spheres, iron complex and anion binding sites. *Reproduced from (Hou et al., 2018) with permission from eLife under Creative Commons Attribution License, (https://creativecommons.org/licenses/by/4.0/)*.

With regard to the functional stoichiometry of the CRAC channel, *D. melaogaster* Orai crystal structure further revealed a hexameric channel complex with a highly Ca^{2+}-selective pore, in contrast to a functional tetramer suggested by various studies with Orai1 concatemers and single-molecule photobleaching (Penna et al., 2008, Mignen et al., 2008, Maruyama et al., 2009). The NMR structure of human Orai1-C-terminus (aa272-292) also supports active hexameric channel in 1:1 complex with STIM1 CC1-CC2 domains (Stathopulos et al., 2013). Later, two studies on Orai1 concatemers argued against a tetrameric assembly and indicated that the Orai1 channel indeed functions as a hexamer (Cai et al., 2016, Yen et al., 2016).

1.2.4 STIM1-Orai1 coupling

Following ER Ca^{2+} depletion, the extended conformation of SOAR or CAD oligomers spans the distance between ER and PM at ER-PM junctions, where they recruit, interact with and activate Orai channels (Yuan et al., 2009, Park et al., 2009, Muik et al., 2011). Structural insights into the C-terminal CC region of STIM1 with/without Orai1 C-terminal fragment revealed that the coupling potentially involves the electrostatic interactions between the basic residues within CC2 or Sα1 region of STIM1 (aa 382-387) and the acidic residues within Orai1 C-terminus (aa 272-291), together with hydrophobic interactions (Yang et al., 2012, Stathopulos et al., 2013). Mutations to neutralize these charged or hydrophobic residues, as well as deletion of STIM1 CC2 domain or Orai1 C-terminus, disrupt coupling to and activation of Orai1 channels (Muik et al., 2008, Calloway et al., 2009, Calloway et al., 2010, Korzeniowski et al., 2010).

Orai1 C-terminus functions synergistically with N-terminus to couple STIM1 binding to channel gating and ion-selectivity (Palty et al., 2015, Palty and Isacoff, 2016, Zhou et al., 2016). STIM1 controls the gating and ion-selectivity of Orai1 channels by interacting with their N-terminal region, consisting of both basic and hydrophobic residues (Li et al., 2007, Muik et al., 2008, Park et al., 2009, Lis et al., 2010, McNally et al., 2013, Derler et al., 2013, Zheng et al., 2013). Besides, the

SOAR dimer cross-links two adjacent subunits of Orai1 hexamer in a unimolecular coupling model to facilitate the channel cooperativity, where Phe^{394} between CC2 and CC3 domains of SOAR is critical for binding to N-terminus and gating of Orai1 (Zhou et al., 2018).

A highly conserved hinge region (aa305-308) connecting TM4 to C-terminus of *D. melanogaster* Orai dimer facilitates the anti-parallel orientation of C-termini at an angle of 152^{o}, supported by the inter-subunit hydrophobic interactions between Ile^{316} and Leu^{319} (Leu^{273} and Leu^{276} in human). Mutations to less hydrophobic residues or deletion of the C-terminus disrupts interactions with STIM1 (McNally et al., 2013, Zheng et al., 2013, Palty et al., 2015, Zhou et al., 2016). The NMR structure of human Orai1-C-terminus bound to STIM1 CC1-CC2 domains revealed the crossing angle of 136^{o} for the C-termini, suggesting STIM1-induced conformational change in Orai C-termini (Stathopulos et al., 2013).

The polybasic lysine-rich C-terminus of STIM1 (aa672-685) can interact with Pro-rich N-terminus of Orai1 to inhibit Orai1 activation and its deletion (STIM1ΔK) promotes Orai1 activation (Yuan et al., 2009). However, STIM1ΔK expressed alone, fails to redistribute into puncta within ER-PM junctions (Liou et al., 2007), but forms puncta when coexpressed with Orai1 and activates I_{CRAC} via its CAD/SOAR domain (Li et al., 2007, Park et al., 2009). Thus, the polybasic tail per se is not essential for Orai1 activation but likely interacts with the PM acidic phospholipids to recruit STIM1 within ER-PM junctions, thereby facilitating binding of CAD/SOAR domain to Orai1 for activation (Korzeniowski et al., 2009, Walsh et al., 2009).

I_{CRAC} is inactivated by rapid Ca^{2+}-dependent inactivation of Orai1, followed by slow dissociation of the STIM1-Orai1 junctional complex. Ca^{2+}-dependent inactivation is mediated by local Ca^{2+} feedback (Zweifach and Lewis, 1995), acidic residues in the STIM1 cytosolic inhibitory domain (aa 475-483) (Mullins et al., 2009, Derler et al., 2009, Lee et al., 2009), calmodulin (Litjens et al., 2004, Mullins et al., 2009) or calmodulin-independent conformational change in Trp^{76} and Tyr^{80} residues within the Orai1 pore (Mullins et al., 2016). The slow dissociation and deoligomerization of the STIM1-Orai1 complex are mediated by an increase in junctional Ca^{2+} and $[Ca^{2+}]_{ER}$ (Shen et al., 2011).

1.2.5 Other associated proteins/channels

Although STIM1 alone can gate Orai1 invitro and reconstitute I_{CRAC} when co-expressed (Zhang et al., 2006, Peinelt et al., 2006, Soboloff et al., 2006b, Zhou et al., 2010a), other associated proteins/channels can modulate the efficiency of I_{CRAC} in native cells and in turn be regulated by STIM1. These interacting partners are summarized in table 1 below.

Table 1. Non-Orai1 partners of STIM1, molecular basis of interactions and functional consequences.

Partner	Location	Interaction	Evidence/ Method	Functional consequences	References
STIM2	ER	Homomerize with STIM1, binds to Orai	Co-immunoprecipitation (Co-IP), total internal reflection fluorescence (TIRF) and confocal microscopy	More sensitive to a small reduction in $[Ca^{2+}]_{ER}$, regulates basal cytosolic Ca^{2+} homeostasis. Coexpression with Orai1 constitutively activates I_{CRAC} and Ca^{2+} influx.	(Soboloff et al., 2006a, Brandman et al., 2007, Zhou et al., 2009, Stathopulos et al., 2009, Subedi et al., 2018)
TRPC channels	PM	Physical binding via ERM of STIM1 and electrostatic interaction between lysine residues of STIM1 and aspartate residues in TRPC	Co-IP, Glutathione S-transferase (GST)-pulldown, whole cell patch clamp, TIRF microscopy	Ca^{2+} and Na^{+} entry; highly tissue- and stoichiometry-dependent role in Ca^{2+} signalling	(Huang et al., 2006, Yuan et al., 2007, Zeng et al., 2008, Cheng et al., 2011, Lee et al., 2014)
Voltage-gated Ca^{2+} channels ($Ca_v1.2$)	PM	CAD of STIM1 and C-terminus of $Ca_v1.2$	Co-IP, Ca^{2+} imaging, whole cell patch clamp, confocal microscopy	Inhibits Ca^{2+} entry via $Ca_v1.2$ after store depletion	(Wang et al., 2010, Park et al., 2010)
Arachidonic acid-regulated calcium (ARC) channels	PM	Constitutive association with C-terminus of PM-resident STIM1	Förster resonance energy transfer (FRET), Co-IP	Store-independent Ca^{2+} entry	(Thompson and Shuttleworth, 2013)
PMCA	PM	Indirect; coupling via partner of STIM1 (POST)	Co-IP, Ca^{2+} imaging	Inhibits Ca^{2+} extrusion from the junctional space	(Ritchie et al., 2012, Krapivinsky et al., 2011)
NCX	PM	Unclear	Whole cell patch clamp	Promotes Ca^{2+} entry	(Liu et al., 2010)
Adenylyl cyclases	PM	Binding between Orai1 and adenylyl cyclase 8 via N-termini	FRET, GST-pulldown, Co-IP	Enhances cyclic adenosine monophosphate (cAMP) production and PKA activation	(Lefkimmiatis et al., 2009, Willoughby et al., 2012)
SOCE-associated regulatory factor (SARAF)	ER	OASF region of STIM1 and cytoplasmic N-terminus of SARAF	TIRF microscopy, Ca^{2+} imaging, Co-IP, whole cell patch clamp	Cytosolic Ca^{2+}-dependent inactivation of Orai	(Palty et al., 2012)

STIM-activating enhancer (STIMATE)	ER	CC1 domain (amino acids 233 – 343) of STIM1 and C-termini of STIMATE	Co-IP, GST-pulldown, Ca^{2+} imaging, FRET analysis	Promotes SOCE and NFAT signalling	(Jing et al., 2015)
Partner of STIM1 (POST)	ER (major), PM (minor)	Coupling with STIM1 upon store depletion	Co-IP, Ca^{2+} imaging, whole cell patch clamp, TIRF microscopy	No effect on SOCE. Promotes STIM1 binding to SERCA2, PMCA, Na^+/K^+-ATPase, and nuclear transporters Importin-β1 and Exportin-1, and attenuates PMCA activity	(Krapivinsky et al., 2011)
Junctate	ER	N terminus of STIM1 and ER-luminal region (residues 71–236) of junctate	Co-IP, GST-pulldown, Ca^{2+} imaging, TIRF microscopy	$[Ca^{2+}]_{ER}$ sensor, structural platform to recruit STIM1 into ER-PM junctions	(Srikanth et al., 2012)
Orosomuc-oid like 3 (ORMDL3)	ER	Unclear	Co-localization via confocal microscopy	Negative modulator of SOCE	(Carreras-Sureda et al., 2013)
ERp57	ER	Two conserved cysteine residues, C49 and C56 of STIM1	Surface plasmon resonance screen, FRET	Negative modulator of SOCE	(Prins et al., 2011)
SERCA	ER	Coupling via phospholamban (PLN). Colocalized with STIM1 into junctions upon ER Ca^{2+} depletion.	FRET, colocalization	Recruited into junctions for ER refilling	(Sampieri et al., 2009, Manjarres et al., 2010)
CRAC regulatory protein 2A, CRACR2A	Cytosol	Ternary complex with Orai1-N-terminus and STIM1 at low junctional Ca^{2+} levels	Co-IP, GST-pulldown, TIRF microscopy	Promotion of SOCE and dissociation of STIM1-Orai1 complex after Ca^{2+} influx	(Srikanth et al., 2010)
Golli	Cytosol	C-terminus of STIM1	GST-pulldown, affinity chromatography, mass spectroscopy	Interaction with STIM1-Orai1 complex to attenuate SOCE upon Ca^{2+} influx after store depletion	(Feng et al., 2006, Walsh et al., 2010)
Calmodulin	Cytosol	N-terminus of Orai1	Co-IP, GST-pulldown	Ca^{2+}-dependent inactivation of Orai1	(Litjens et al., 2004, Mullins et al., 2009)
Septins	PM	Binds PIP2	Ca^{2+} imaging, TIRF microscopy	Reorganize PIP2 within ER-PM junctions and facilitate STIM1-Orai1 recruitment	(Sharma et al., 2013)

Reproduced from (Groschner et al., 2018) with permission from Taylor & Francis Group, LLC under Creative Commons Attribution-NonCommercial-NoDerivs 3.0 Unported License (https://creativecommons.org/licenses/by-nc-nd/3.0/). Note: Additional interacting partners are included.

1.2.3 (Patho)physiological role in Ca^{2+} signaling

SOCE is a major Ca^{2+} influx pathway in the non-excitable cells, including immune cells and secretory epithelial cells (Soboloff et al., 2012). Physiological stimulation of cell-surface receptors promotes cyclic ER Ca^{2+} release via IP_3R/RyR and reuptake via SERCA, resulting in cytosolic Ca^{2+} oscillations (Dupont et al., 2011). The Ca^{2+} oscillations vary in frequency and amplitude, which determines the specificity and efficiency of gene expression in B-and T-cells (Dolmetsch et al., 1997, Dolmetsch et al., 1998). SOCE sustains these oscillatory Ca^{2+} signals via

replenishing the depleted Ca^{2+} stores and counteracting Ca^{2+} efflux through PM Ca^{2+} pumps. Without influx, Ca^{2+} stores cannot refill and the oscillations run down and cease (Wedel et al., 2007, Boie et al., 2017).

Following SOCE in immune cells, Ca^{2+}-calmodulin complex activates calcineurin, which then dephosphorylates NFAT. The dephosphorylated NFAT translocates from cytosol to nucleus and regulates downstream expression of cytokines, transcription factors, and enzymes, which in turn govern various cellular processes in immune cells such as proliferation, differentiation, metabolism, mast cell degranulation, and cytotoxicity (Vaeth and Feske, 2018). Moreover, the local Ca^{2+} signal (Ca^{2+} microdomain) near open CRAC channels, rather than the global Ca^{2+} oscillation itself, governs *c-fos* gene expression, NFAT1 activation in mast cells (Di Capite et al., 2009, Kar et al., 2011). During each oscillation spike coupled with transient ER Ca^{2+} drop, STIM1, rather than STIM2, translocates dynamically into ER-PM junctions and activates junctional Ca^{2+} entry (Bird et al., 2009), which provides digitized Ca^{2+} signals for regulation of gene expression following stimulation of cysteinyl leukotriene type I receptors in mast cells (Kar et al., 2012). However, stimulation of tyrosine kinase-coupled FCεRI receptors in the same cells drives gene expression through junctional recruitment of both STIM1 and STIM2 (Kar et al., 2012).

Deletion/mutation of genes in mice and other models implicate the role of SOCE in skeletal muscles. Skeletal muscles consist of triad junctions, where a transverse tubule is sandwiched between two SR terminal cisternae. Mechanical coupling between $Ca_v1.1$ in the transverse tubule and RyR1 in the SR terminal cisternae mediates EC coupling in the skeletal muscles (Michelucci et al., 2018). Various tissues, including skeletal and cardiac muscles, brain, spleen, lungs, and liver consist of two functionally distinct variants of STIM1: 115-kDa STIM1L and 90-kDa STIM1S (Darbellay et al., 2011). STIM1L interacts with actin and pre-localizes as clusters in the SR terminal cisternae, close to Orai1 in the transverse tubule within the triad junctions. In such a pre-localized setting, SOCE can be quickly activated via repetitive, transient Ca^{2+} depletion within SR terminal cisternae during EC coupling, bypassing STIM1 redistribution and SR remodeling (Darbellay et al., 2011, Koenig et al., 2019). On the other hand, STIM1S is diffusely distributed in non-junctional SR at I-band at rest and recruited slowly into junctions following store depletion to mediate additional graded SOCE (Darbellay

et al., 2011). During exercise involving rapid, repetitive action potentials, transverse tubule elongates to form new junctions with SR within the I-band, so that STIM1S interacts with Orai1, rather than translocation of STIM1 oligomers into ER-PM junctions, as seen in non-excitable cells. This promotes SOCE, which boosts muscle contractility and resists fatigue (Boncompagni et al., 2017).

STIM1/Orai1-mediated SOCE further regulates long-term muscle development and differentiation into fatigue-resistant fibers through activation of downstream Ca^{2+}-dependent transduction pathways (Stiber et al., 2008, Li et al., 2012, Carrell et al., 2016). Global or muscle-specific STIM1 knockout in mice abolishes SOCE, reduces SR Ca^{2+} content, and hinders muscle development, leading to myopathy and death before adulthood (Stiber et al., 2008, Li et al., 2012, Seth et al., 2012). Constitutive, muscle-specific knockout of Orai1 (Carrell et al., 2016) or muscle-specific expression of dominant-negative Orai1 (E106Q) (Wei-Lapierre et al., 2013, Lyfenko and Dirksen, 2008) abolishes SOCE, which enhances susceptibility to fatigue during repetitive stimulation and hinders muscle development.

Patients with inherited loss-of-function mutations in STIM1 and/or Orai1 suffer from CRAC channelopathy, characterized by combined immunodeficiency, skeletal muscle hypotonia, thrombocytopenia, and ectodermal dysplasia (Vaeth and Feske, 2018, Michelucci et al., 2018). On the other hand, gain-of-function mutations result in constitutive channel activity and manifest in tubular aggregate myopathy, Stormorken and York platelet syndromes, characterized by progressive muscle weakness, thrombocytopenia, and hyposplenism (Michelucci et al., 2018). Furthermore, impaired SOCE contributes to the pathogenesis of muscular dystrophy, malignant hyperthermia, and sarcopenia (Michelucci et al., 2018). Thus, tight regulation of SOCE is critical for the normal physiology of immune cells and skeletal muscles in humans.

Although the role of SOCE in cardiovascular physiology is not fully understood, initial studies indicated its involvement in agonist-induced NFAT translocation and hypertrophy in embryonic and neonatal cardiomyocytes in mice, which declines with development (Hunton et al., 2002, Uehara et al., 2002, Hunton et al., 2004). Following identification of STIM and Orai, in vitro/in vivo models focused on their expression and function in cardiac development and physiology. Like skeletal muscles, neonatal cardiomyocytes express STIM1L in addition to

regular STIM1 variant, but the expression declines with development (Luo et al., 2012). STIM1/Orai1 knockdown attenuates agonist-induced SOCE and hypertrophic signaling in neonatal rat ventricular cardiomyocytes in vitro (Voelkers et al., 2010, Hulot et al., 2011, Luo et al., 2012). STIM1 is upregulated in the adult rodent hearts following pathological stress like pressure overload-induced hypertrophy, and its knockdown ameliorates the condition (Hulot et al., 2011, Luo et al., 2012, Parks et al., 2016, Benard et al., 2016). Cardiomyocyte-specific STIM1 knockout doesn't affect early development in mice but later results in SR and mitochondrial abnormalities, reduced contractility, dilated cardiomyopathy, and cardiac fibrosis (Collins et al., 2014, Parks et al., 2016). Orai1 deficient ($Orai1^{+/-}$) mice also develop dilated cardiomyopathy and die of heart failure (Horton et al., 2014).

On the other hand, transgenic mice with overexpressed STIM1, to mimic upregulation under pathological conditions, are healthy in early life, but young cardiomyocytes display enhanced spontaneous Ca^{2+} transients and Ca^{2+} spark frequency in response to pressure overload or agonist stimulation. Later, adult cardiomyocytes display increased diastolic Ca^{2+}, transient amplitude, and downstream transcription coupling although SR Ca^{2+} content is unaltered. Impaired Ca^{2+} signaling leads to hypertrophy, cardiac failure, arrhythmia, and eventually sudden death (Correll et al., 2015). In contrast, transient STIM1 overexpression in adult rat ventricular cardiomyocytes enhanced SR Ca^{2+} content and leak by binding PLN and indirectly activating SERCA2a, rather than SOCE (Zhao et al., 2015). Endogenous STIM1 forms puncta upon store depletion in neonatal rat cardiomyocytes (Hulot et al., 2011), but in adult rat ventricular cardiomyocytes, STIM1 appears in puncta-like structures in junctional SR and store depletion doesn't facilitate further redistribution (Zhao et al., 2015). Moreover, overexpressed STIM1 is slightly pre-clustered at rest and may aggregate further upon store depletion (Parks et al., 2016), though the slow mobilization rate is unaltered (Zhao et al., 2015). In addition to Orai1, STIM1 can interact with a number of proteins/channels to modulate intracellular Ca^{2+} signaling in cardiovascular cells under normal and pathological conditions (Figure 9, Table 1).

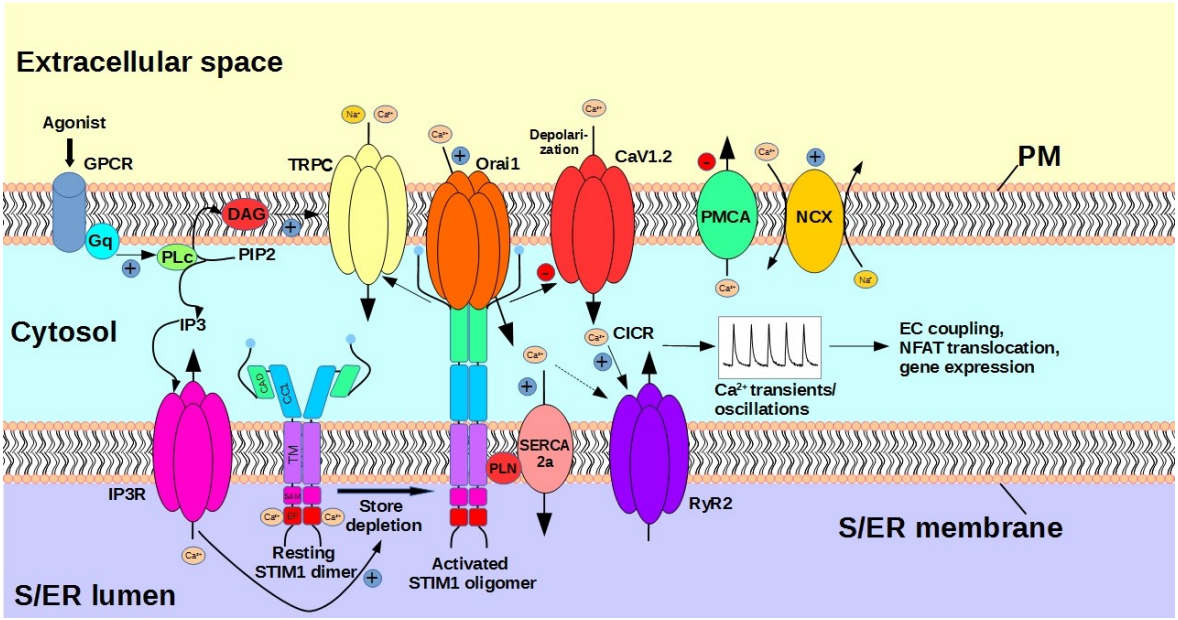

Figure 9. Effectors/interaction partners of STIM1 and mechanisms associated with SOCE in cardiovascular cells.

Upon depolarization, Ca^{2+} influx through $Ca_v1.2$ triggers Ca^{2+}-induced Ca^{2+} release (CICR) from SR stores through RyR2. Cytosolic Ca^{2+} is sequestered via SR reuptake through SERCA2a or efflux through PM Ca^{2+} channels; NCX or PMCA. Following agonist activation of G protein-coupled receptors (GPCR), PLC is activated to convert PIP2 to DAG and IP_3. While DAG activates TRPC channels, IP_3 stimulates SR Ca^{2+} release via IP_3R so that STIM1 loses bound Ca^{2+} at EF-hand, oligomerizes, translocates into SR-PM junctions, and activates Orai1 or inhibits $Ca_v1.2$ channels. In addition to SR refilling, Orai1-mediated Ca^{2+} influx appears essential for oscillatory Ca^{2+} cycling, NFAT translocation, and gene expression. STIM1 also activates SERCA2a via PLN, inhibits PMCA, and regulate TRPC channels and reverse mode NCX. *Reproduced from (Groschner et al., 2017) with permission from Springer Nature (Order number: 4576441232950).*

STIM1 and Orai1 are also expressed in sinoatrial node cells involved in cardiac automaticity since cardio-specific STIM1 knockout in mice or SOCE blockers attenuate Ca^{2+} influx, spontaneous Ca^{2+} transients, SR Ca^{2+} content, and heart rate (Zhang et al., 2015, Liu et al., 2015). Besides, the aorta of spontaneously hypertensive rats has higher expression of STIM1 and Orai1, and displays elevated basal tonus and contraction in response to thapsigargin-induced Ca^{2+} influx, which is attenuated by SOCE blockers or antibodies against STIM1/Orai1 (Giachini et al., 2009). Moreover, STIM1 is upregulated following angiotensin II-induced hypertension in mice, characterized by cardiac hypertrophy, ER stress-induced vascular dysfunction, and reduced phosphorylation of

endothelial nitric oxide synthase, whereas smooth muscle-specific knockout of STIM1 ameliorates these cardiovascular pathologies (Kassan et al., 2016).

1.3 Aim

A number of previous studies have proposed TRICA as a unique $[Ca^{2+}]_{ER}$ sensing cation channel involved in facilitating $[Ca^{2+}]_{ER}$ release and regulating intracellular K^+/Ca^{2+} homeostasis. TRICA has been postulated to modulate RyR-mediated oscillatory Ca^{2+} signaling, though the underlying mechanistic role remains elusive.

The aim of this thesis work was to characterize the role of TRICA in the context of RyR2-mediated spontaneous Ca^{2+} oscillations. Using a simple human embryonic kidney cell model, stably expressing RyR2 (HEK293_RyR2 cells), which mimics a cardiac Ca^{2+} signaling phenotype, we planned to decipher the cellular and molecular mechanism(s) that link ER and PM function to achieve frequency modulation of Ca^{2+} signaling.

2. Materials and methods

2.1 Reagents and constructs

All reagents used were of molecular biology grade, purchased from Sigma-Aldrich unless specified otherwise. HEK293_RyR2 cells and D1ER construct were provided by Roland Malli (Medical University of Graz, Austria). We cloned TRICA-mCherry in pEYFP-N1 vector (Clontech, France) from untagged TRICA, provided by Hiroshi Takeshima (Kyoto University, Japan). YFP-STIM1, Orai1-CFP, myc-STIM1, and mCherry-ER3 were obtained from Indu Ambudkar (NIH, Bethesda, USA). STIM1-CFP, YFP-Orai1, and YFP-STIM1-D76A were provided by Christoph Romanin (University of Linz, Austria).

2.2 Cell culture and transfection

HEK293 cells were cultured in DMEM supplemented with 10% FBS (Gibco 10270), 10 mM HEPES, 1 % penicillin/streptomycin and HEK293_RyR2 cells in the same medium with 250 µg/ml geneticin and 5 µg/ml puromycin instead of penicillin/streptomycin and maintained in an incubator at 37^{o}C, 5% CO_2. The cells at 50-60% confluence in 35 mm-dishes were transiently transfected for 6 h with required constructs, as indicated in the text, using FugeneHD (Promega, Germany) or Lipofectamine 2000 (Invitrogen, Austria) as per manufacturer's instructions. Control cells were mock transfected with an ER marker, mCherry-ER3 plasmid. Experiments were performed 40–48 h after transfection.

2.3 $[Ca^{2+}]_i$ Imaging and FRET

Changes in intracellular Ca^{2+} levels, $[Ca^{2+}]_i$ was monitored using Fura-2 ratiometric imaging, as described previously (Di Giuro et al., 2017). Briefly, cells on coverslips were loaded with 1 µM Fura-2 AM for 30 min in an experimental buffer, composed of (in mM): 137 NaCl, 5 KCl, 2 $CaCl_2$, 1 $MgCl_2$, 10 glucose, and 10 HEPES, pH adjusted to 7.4 with NaOH. The coverslip was then mounted in a perfusion chamber on an inverted microscope (Olympus IX71, Germany) with a 20×/0.75 objective and perfused with indicated solutions at 37^{o}C. During the recordings using Live Acquisition v2.6 software (FEI, Germany), cells were excited alternately at 340 and 380 nm using an Oligochrome excitation system (FEI, Germany) and

fluorescent images were captured at 510 nm every 1.2 s with an ORCA-03G digital CCD camera (Hamamatsu, Germany). The 340/380 ratio was used as an index of cytosolic Ca^{2+} levels. ER luminal Ca^{2+} levels, $[Ca^{2+}]_{ER}$ were monitored in cells transfected with CFP/YFP FRET-based D1ER sensor, as described previously (Palmer et al., 2004). Briefly, the emission ratio at 535/470 nm was recorded upon excitation at 430 nm, using an additional OptoSplit II (Cairn Research, UK) in the above Fura-2 imaging setup. Dynamic FRET between STIM1-CFP and YFP-Orai1 was measured using the same setting used for D1ER.

2.4 TIRF Microscopy

TIRF microscopy was performed using an Olympus IX81 motorized inverted microscope (Olympus, MA, USA) with a TIRF-optimized Olympus Plan APO 60x/1.45 oil immersion objective and Lambda 10-3 filter wheel (Sutter Instruments, CA, USA) containing 480/40, 540/30 and 575lp emission filters (Chroma Technology, VT, USA), as described previously (Ong et al., 2015). CFP, YFP, and mCherry were excited by 445, 514 and 561 nm lasers respectively via cell^TIRF Control 1.3 software (Olympus, MA, USA). Images were collected every 5 s using Hamamatsu ORCA-Flash4.0 camera (Olympus, MA, USA) and MetaMorph software (Molecular Devices, MA, USA). Cells plated on poly-l-lysine-coated glass-bottom dishes (MatTek Corporation, MA, USA) were perfused with indicated solutions at 37^{o}C during image acquisition. The fluorescence, colocalization, size, distribution, and rate of clustering of proteins were analyzed using ImageJ 1.51n.

2.5 Whole-cell patch-clamp recording

Patch-clamp recordings were performed in whole-cell configuration, as described previously with modification (Hoth and Penner, 1992, Frischauf et al., 2015, Tiapko et al., 2019). HEK293 cells on coverslips were mounted in a perfusion chamber on an inverted microscope (Zeiss Axiovert 200, Germany) with 40×/0.75 objective and perfused with bath solution at 22-25^{o}C, containing (in mM): 120 NaCl, 2.8 KCl, 0.5 or 10 $CaCl_2$, 1 $MgCl_2$, 20 TEA-Cl, 10 glucose and 10 HEPES, pH adjusted to 7.4 with NaOH. Cells co-expressing YFP-STIM1 and Orai1-CFP were selected using an Oligochrome excitation system and Oligocon v1.1.14 software (FEI, Germany). For passive store depletion, the patch pipette was pulled using P-1000

micropipette puller (Shutter Instrument, CA, USA) and filled with the intracellular solution containing (in mM): 130 K-gluconate, 8 NaCl, 5 $MgCl_2$, 10 HEPES and 20 EGTA, pH 7.2 with KOH and had a resistance of 2-3 MΩ. An Ag/AgCl electrode was used as a reference. Using an Axopatch 200B amplifier and a Clampex v11.0.1 software (Molecular Devices, CA, USA), the pipette capacitance was compensated and current was recorded during voltage ramps ranging from -90 to +90 mV over 1 s, applied every 5 s from a holding potential of 0 mV, filtered at 2 kHz and digitized at 10 kHz using Digidata 1440A (Molecular Devices, CA, USA). In Clampfit v11.0.1, the current recorded during the first few ramps was used for leak subtraction of the subsequent current recordings. All voltages were corrected for a liquid junction potential of 13.5 mV between the bath and pipette solutions and I_{CRAC} was measured at -80 mV.

2.6 Co-immunoprecipitation (Co-IP) and Western blot

Cells were washed with 1×PBS and lysed in ice-cold Pierce IP lysis buffer supplemented with protease inhibitor cocktail (ThermoFisher Scientific, NY, USA). Cell lysates were centrifuged (10,000 g, 10 min at 4°C) and quantified by Pierce BCA protein assay kit (ThermoFisher Scientific, NY, USA). Co-IP experiments were done using Pierce Anti-c-myc magnetic beads (ThermoFisher Scientific, NY, USA) as per manufacturer's instructions. The immunoprecipitants were eluted in NuPAGE LDS sample buffer (Invitrogen, NY, USA) with 5% DTT by heating at 95 °C for 10 min. The proteins were resolved in NuPAGE 4–12% Bis-Tris gel (Invitrogen, NY, USA) and transferred to 0.2 µm PVDF membranes using the Trans-Blot Turbo Transfer System (Biorad, CA, USA). Membranes were blocked with 5% (w/v) non-fat milk in Tris-buffered saline containing 0.1% Tween 20 (TBST, 25^{o}C, 1 h) and incubated with primary antibodies overnight at 4^{o}C. The following primary antibodies (diluted in 5% [w/v] bovine serum albumin-TBST) were used: myc (1:1000, 2276, Cell Signaling, MA, USA), STIM1 (1:1000, 4916, Cell Signaling, MA, USA), Orai1 (1:1000, produced against C-terminal epitope ELAEFARLQDQLDHRGD and affinity purified by Lofstrand Labs Limited (Gaithersburg, MD, USA)), TMEM38A (1:200, sc-390054, Santa Cruz, TX, USA) and β-actin (1:2500, ab8224, Abcam, MA, USA). After washing, the membranes were incubated with HRP-conjugated goat anti-mouse IgG or goat anti-rabbit IgG (1:10,000, Jackson Immunoresearch, PA, USA) (25^{o}C, 1 h). Immunoreactive

bands were visualized using SuperSignal West Pico Chemiluminescent Substrate (ThermoFisher Scientific, NY, USA) in ChemiDoc MP Imaging System (Biorad, CA, USA) and densitometric evaluation was performed using Image Lab 6.0 software (Biorad, CA, USA).

2.7 Data analysis

Data analyses were performed using OriginPro 2015 (OriginLab, MA, USA) and Prism 5 (GraphPad Software, Inc., CA, USA). Data are expressed as mean ± SEM. n represents the number of cells from at least three independent experiments unless specified otherwise. Approximate normal distribution of data was assessed by z-value of skewness and kurtosis and D'Agostino-Pearson omnibus normality test. Unless specified otherwise, unpaired t-test was used to test the statistical significance for normally distributed data (with Welch's correction for significantly different variances between groups), otherwise Mann-Whitney rank test was applied. χ^2 test was used to analyze responses in cell populations. All tests were two-tailed and p values <0.05 were considered significant.

3. Results

3.1 TRICA modifies the frequency and amplitude of RyR2-mediated oscillations

HEK293_RyR2 cells offer an established model of relatively simple molecular composition to mimic the cardiac phenotype for studying RyR2-induced spontaneous Ca^{2+} oscillations, known as store-overload-induced Ca^{2+} release (SOICR) (Jiang et al., 2004). These oscillations occur due to SR Ca^{2+} overload in cardiac cells under various conditions, namely elevated extracellular Ca^{2+} ($[Ca^{2+}]_o$), ischemia/reperfusion, digitalis toxicity, and independently of membrane depolarization (Lakatta, 1992). Raising $[Ca^{2+}]_o$ increases the steady-state ER Ca^{2+} content in HEK293_RyR2 cells, thereby promoting the discharge of the Ca^{2+} stores via RyR2, which are at the same time governed by local Ca^{2+} levels (Jiang et al., 2004).

We first accessed the effect of TRICA on SOICR-associated oscillatory Ca^{2+} signals by transient expression of TRICA-mCherry in HEK293_RyR2 cells that do not express TRICA endogenously (Figure 10A). Cytosolic Ca^{2+} oscillations were recorded in response to $[Ca^{2+}]_o$ elevations from nominally free to 0.1, 0.3 and 1.0 mM (Figure 10B). As expected, the frequency of Ca^{2+} oscillations in HEK293_RyR2 cells positively correlated with $[Ca^{2+}]_o$. Expression of TRICA-mCherry significantly reduced the frequency of oscillations to about 50-68% at each $[Ca^{2+}]_o$ when compared to the respective controls (Figure 10C). This frequency modulation by TRICA was associated with a moderately but significantly enhanced average peak amplitude at 1 mM $[Ca^{2+}]_o$ (Figure 10D). Moreover, expression of TRICA-mCherry significantly reduced the proportion of oscillating cells in response to step-wise $[Ca^{2+}]_o$ elevations (Figure 10E). To test whether the Ca^{2+} influx that mediates these cytosolic Ca^{2+} oscillations is via SOCE pathway, HEK293_RyR2 cells were pre-incubated with the SOCE inhibitor, N-[4-[3,5-Bis(trifluoromethyl)pyrazol-1-yl]phenyl]-4-methylthiadiazole-5-carboxamide (BTP2, 10 min) (Zitt et al., 2004). BTP2 indeed completely blocked these oscillations (Figure 10B), suggesting SOCE could be the major Ca^{2+} influx pathway for refilling ER Ca^{2+} stores and initiating Ca^{2+} discharge during the oscillatory cycle.

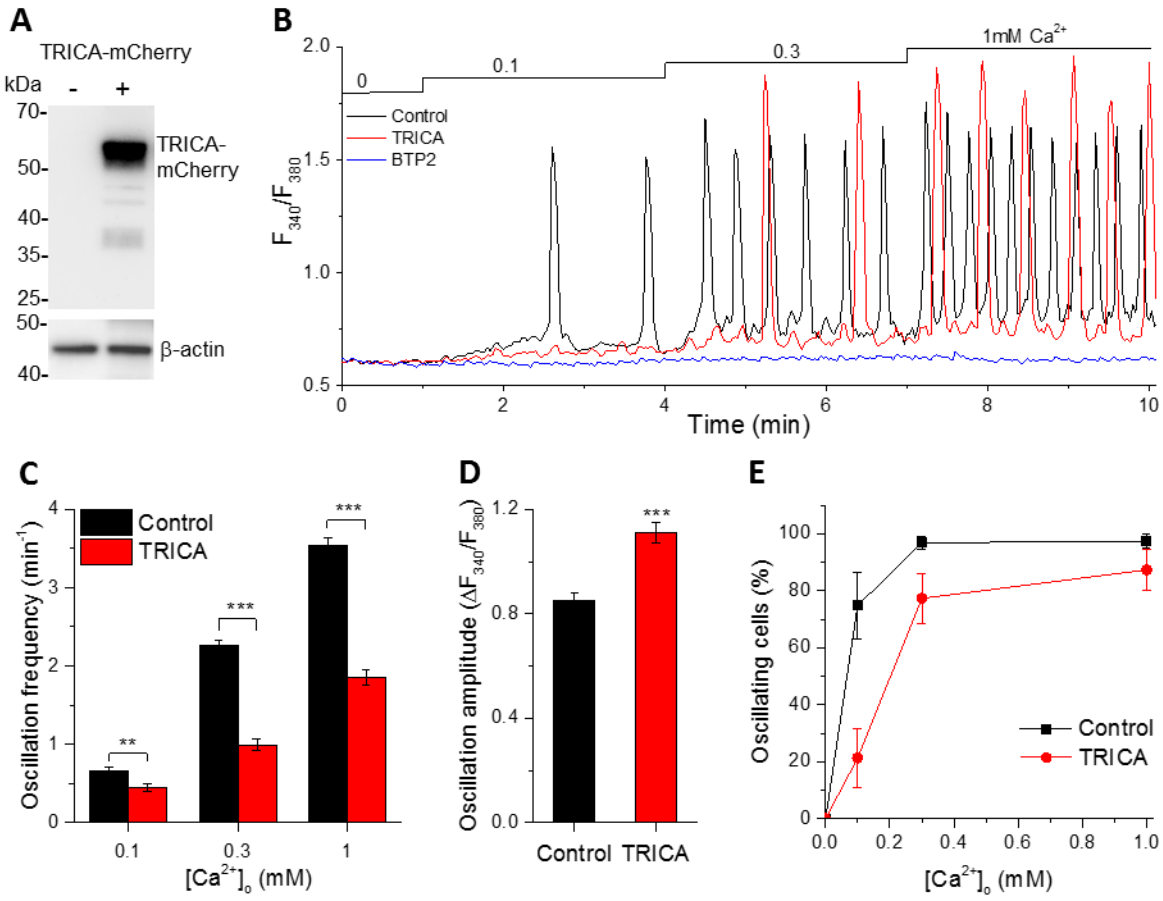

Figure 10. TRICA modifies the frequency and amplitude of RyR2-mediated cytosolic Ca^{2+} oscillations.

(A) Representative Western blot showing an absence of endogenous TRICA bands at ~33 kDa using anti-TRICA antibody in wild-type (-) and TRICA-mCherry transfected (+) HEK293 cells, n=3 independent experiments. **(B)** Traces of cytosolic Ca^{2+}-sensitive Fura2 ratio, representing SOICR-associated oscillations in mCherry-ER3 (control, black) or TRICA-mCherry transfected (TRICA, red) HEK293_RyR2 cell and lack of oscillations in 3 μM BTP2-incubated (BTP2, blue) control cell. **(C)** Ca^{2+} oscillation frequency at 0.1, 0.3 and 1 mM $[Ca^{2+}]_o$, **(D)** amplitude at 1 mM $[Ca^{2+}]_o$ and **(E)** proportion of oscillating cells in TRICA cells (n=88) vs. controls (n=81); **p<0.01, ***p<0.001; mean ± SEM values are shown.

Besides cytosolic Ca^{2+} responses, we measured Ca^{2+} oscillations within the ER lumen using a genetically encoded ER-targeted Ca^{2+} sensor D1ER (Palmer et al., 2004) (Figure 11A). The frequency of Ca^{2+} oscillations within the ER lumen of HEK293_RyR2 cells was also positively correlated with increasing $[Ca^{2+}]_o$, and TRICA-mCherry expression significantly reduced the frequency of ER Ca^{2+} signals by about 50% at each $[Ca^{2+}]_o$ as compared to controls (Figure 11B), probably due to reduced sensitivity of RyR2 to luminal Ca^{2+}. TRICA-mCherry expression

enhanced the average peak amplitude of individual ER Ca^{2+} depletion events (Figure 11C shows quantification at 1 mM $[Ca^{2+}]_o$). Moreover, TRICA-mCherry expression clearly increased the time required to obtain complete ER Ca^{2+} refilling (Figure 11A). Hence, the prominent phenotype of TRICA overexpression was decelerated ER Ca^{2+} refilling and profound prolongation of the cycle length between discharge events. As noted in figure 10A, SOICR-associated ER Ca^{2+} oscillations were also completely abrogated by treatment of cells with BTP2 (Figure 11A).

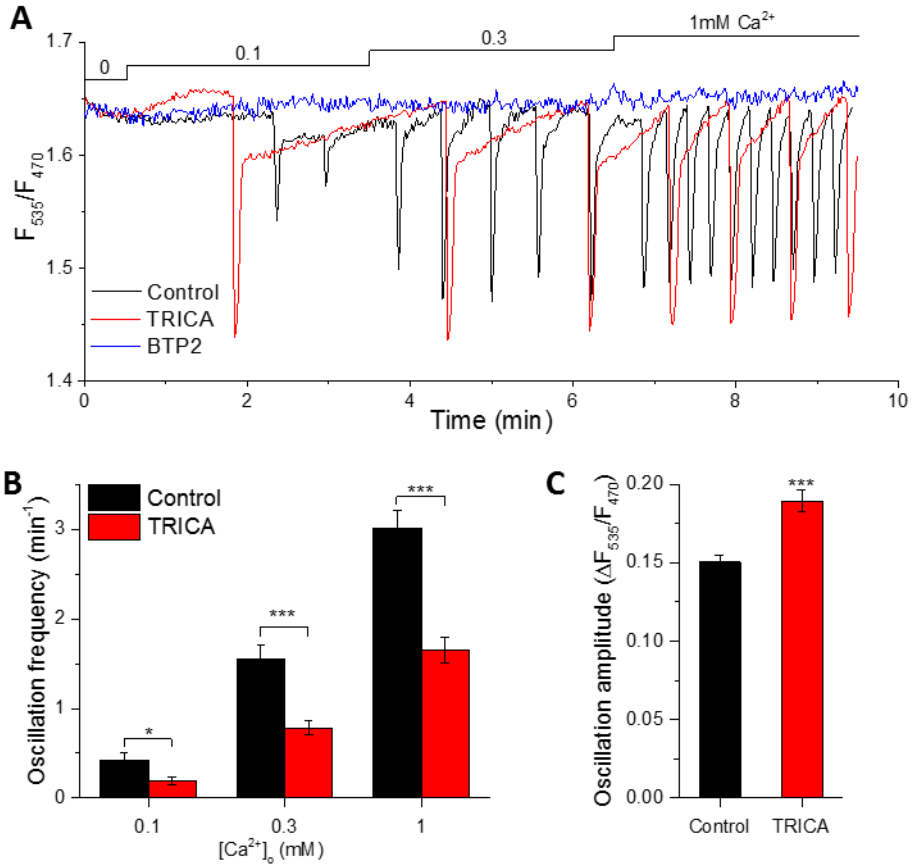

Figure 11. TRICA modifies the frequency and amplitude of RyR2-mediated ER luminal Ca^{2+} oscillations.

(A) Traces of $[Ca^{2+}]_{ER}$-sensitive D1ER FRET ratio, representing SOICR-associated oscillations in mCherry-ER3 (control, black) or TRICA-mCherry transfected (TRICA, red) cell and lack of oscillations in 3 μM BTP2-incubated (BTP2, blue) control cell. **(B, C)** Bars represent mean ± SEM for (B) Ca^{2+} oscillation frequency at 0.1, 0.3 and 1 mM $[Ca^{2+}]_o$ and (C) amplitude at 1 mM $[Ca^{2+}]_o$ in TRICA (+) cells (n=32) vs. controls (n=23); *p<0.05, ***p<0.001.

3.2 TRICA attenuates SOCE irrespective of RyR2-triggered store depletion

Since our findings illustrated in figures 10 and 11 suggest that SOCE may be involved in regulating SOICR in HEK293_RyR2 cells, we investigated whether TRICA modulates SOCE by a standard store-depletion/Ca^{2+} re-addition protocol in HEK293_RyR2 cells. As shown in figure 12A, ER Ca^{2+} release was evoked by the RyR agonist, caffeine, together with the SERCA inhibitor, 2,5-Di-t-butyl-1,4-benzohydroquinone (BHQ) to prevent ER refilling in a nominally Ca^{2+}-free external buffer, followed by re-addition of 1 mM $CaCl_2$ to the medium to measure Ca^{2+} entry. In this setting, TRICA expression promoted Ca^{2+} release from the ER (Figure 12B). Importantly, it induced a significant reduction in the rate of Ca^{2+} influx, the peak amplitude, and sustained $[Ca^{2+}]_i$ elevation by 40%, 47% and 41% respectively (Figures 12C, 12D).

These effects of TRICA expression on SOCE were similar when ER Ca^{2+} was depleted with BHQ alone (without caffeine) in these cells (Figure 12E). The influx rate and amplitudes of peak and sustained cytosolic Ca^{2+} elevation were also significantly reduced by 25%, 20% and 16% respectively (Figures 12F, 12G). Peak cytosolic Ca^{2+} levels in response to BHQ-mediated store depletion were slightly higher in TRICA-expressing cells, although the difference was not statistically significant (Figure 12H). These novel findings suggest that TRICA attenuates the SOCE pathway via a mechanism that is unrelated to ER Ca^{2+} recycling.

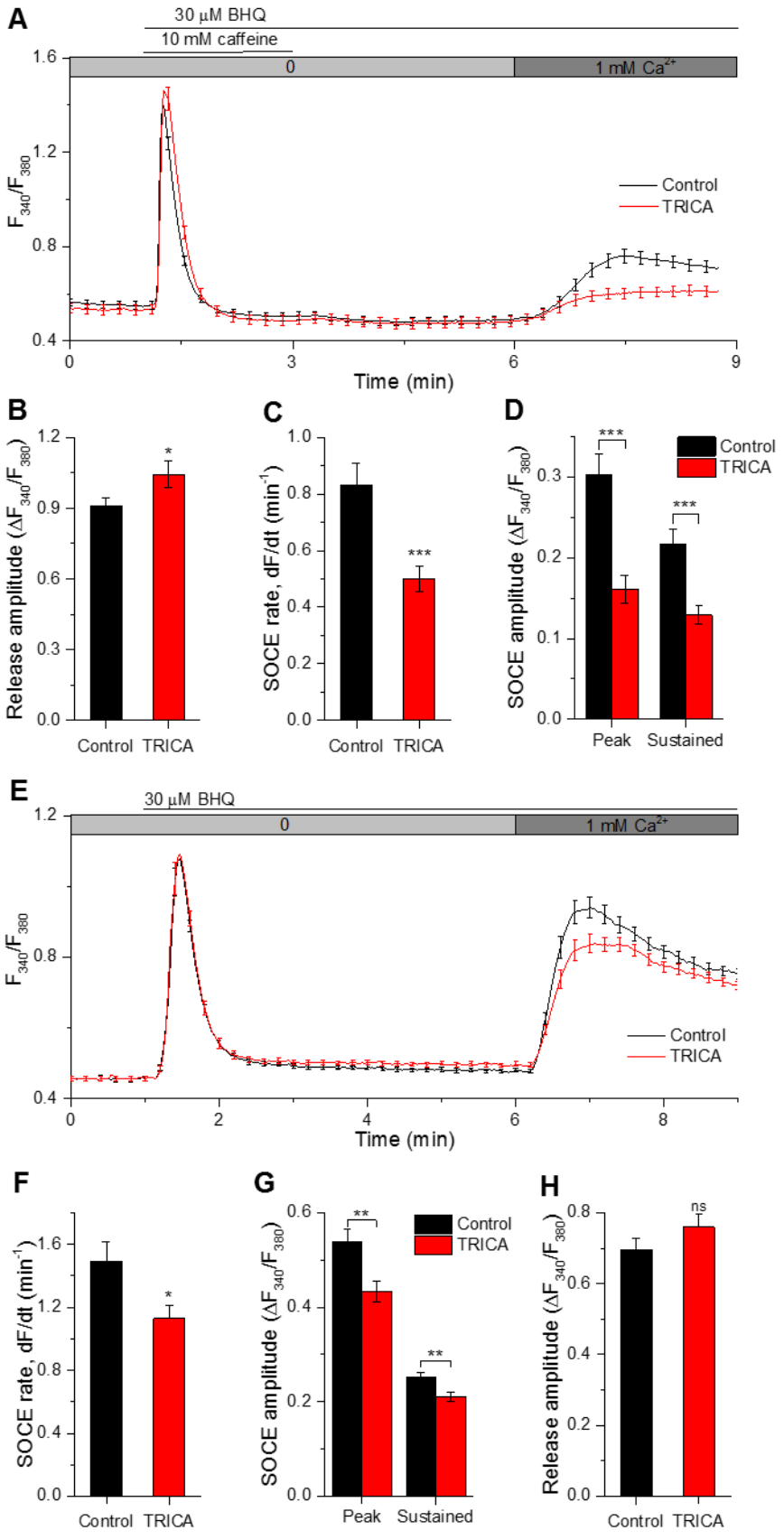

Figure 12. TRICA attenuates SOCE irrespective of RyR2-triggered store depletion.

(A, E) Average cytosolic Ca^{2+}-sensitive Fura-2 traces in mCherry-ER3 (control, black) or TRICA-mCherry (TRICA, red) transfected cells, showing SOCE after ER Ca^{2+} depletion with (A) 10 mM caffeine+30 µM BHQ and (E) 30 µM BHQ. Bars show mean ± SEM for **(B, H)** ER Ca^{2+} release peak amplitude, **(C, F)** SOCE rate and **(D, G)** peak and sustained SOCE amplitude in TRICA (+) (n (A)=42, n (E)=52) vs. control (n (A)=49, n (E)=54)) cells; *p<0.05, **p<0.01, ***p<0.001, ns (non-significant).

3.3 TRICA attenuates SOCE irrespective of RyR2 expression and without affecting STIM1 and Orai1 expression

These effects of TRICA expression on SOCE were further tested by examining agonist-stimulated Ca^{2+} signals in wild-type HEK293 cells that lack RyR2 expression (Figure 13A). Peak increases in $[Ca^{2+}]_i$ in response to stimulation with PLC-coupled receptor agonist, carbachol (CCh) and BHQ were not significantly altered by TRICA expression (Figure 13B), indicating that ER Ca^{2+} release remains unaffected under these conditions. However, as previously observed in figure 12A, the rate of Ca^{2+} entry, as well as peak and sustained $[Ca^{2+}]_i$ elevations, were significantly inhibited by 35%, 39%, and 33% respectively by TRICA expression (Figures 13C, 13D).

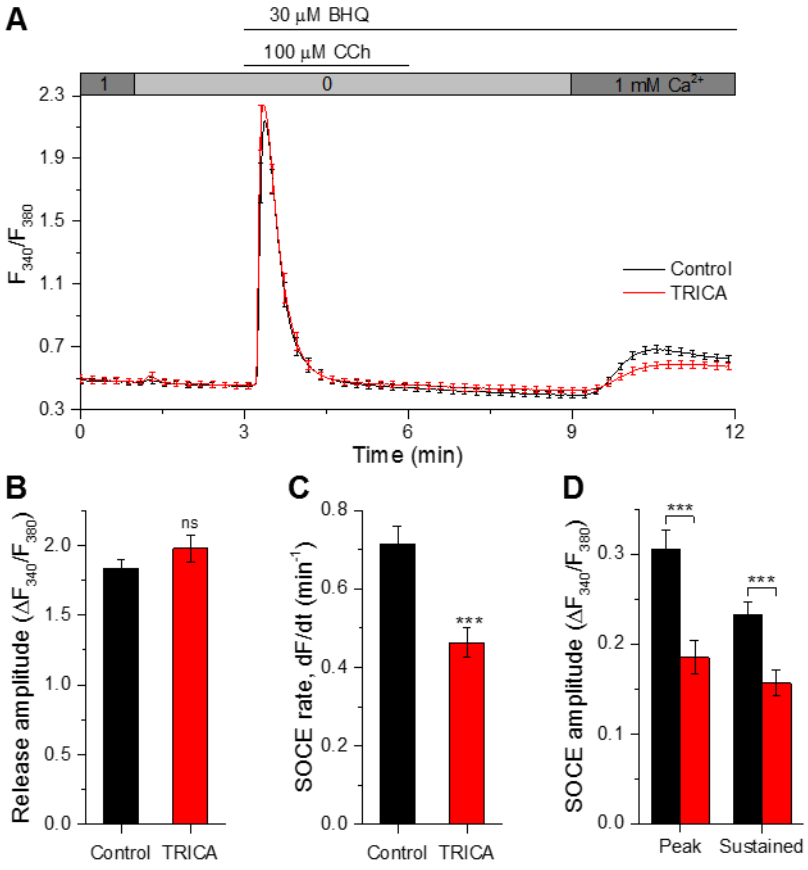

Figure 13. TRICA attenuates SOCE irrespective of RyR2 expression.

(A) Average cytosolic Ca^{2+}-sensitive Fura-2 traces in mCherry-ER3 (control, black) or TRICA-mCherry (TRICA, red) transfected wild-type HEK293 cells, showing SOCE after ER Ca^{2+} depletion with 100 µM CCh+30 µM BHQ. **(B-D)** Bars show (B) ER Ca^{2+} release peak amplitude, (C) SOCE rate and (D) peak and sustained SOCE amplitude in (A) TRICA (+) (n=30) vs. control (n=38) cells; ***p<0.001, ns (non-significant).

Importantly, SOCE attenuation in TRICA-expressing cells was not due to diminished expression of its two major molecular components, STIM1 and Orai1, as confirmed by immunoblotting (Figures 14A, 14B).

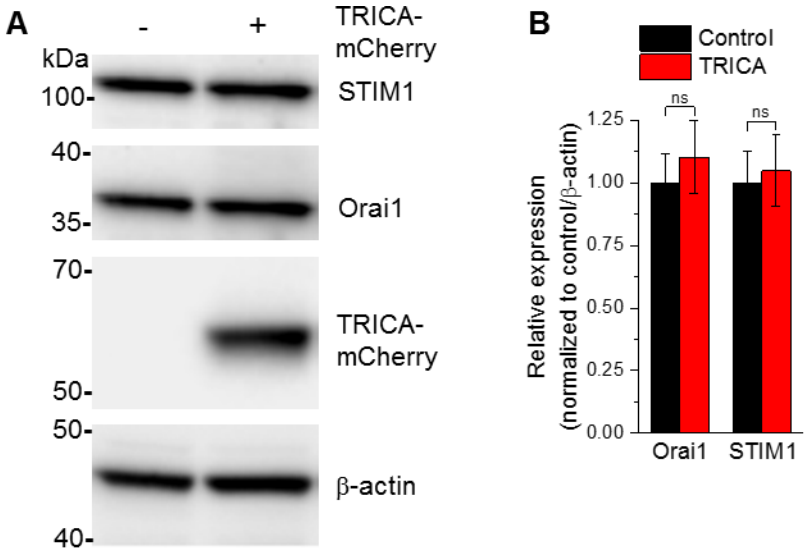

Figure 14. TRICA does not affect STIM1 and Orai1 expression in HEK293 cells.

(A) Representative Western blots for STIM1, Orai1, TRICA-mCherry expression in control and TRICA-mCherry transfected cells with β-actin as a loading control, n=6 independent experiments. **(B)** Densitometric evaluation of immunoreactive bands of Orai1 and STIM1 shown in (A), ns (non-significant).

3.4 TRICA dampens SOCE-associated $[Ca^{2+}]_i$ responses to low and high stimuli levels

In an attempt to elucidate the impact of TRICA expression on agonist-dependent Ca^{2+} signaling responses, sustained via SOCE, we investigated $[Ca^{2+}]_i$ responses in HEK293 cells at various [CCh]. As reported previously (Ong et al., 2015), CCh-induced $[Ca^{2+}]_i$ responses varied with an increase in stimulus intensities, with baseline Ca^{2+} oscillations at low [CCh] and sustained elevations at maximal [CCh]. We observed TRICA-induced variation in the Ca^{2+} signaling pattern at each [CCh]. We categorized these responses into four groups between 6 and 10 min time frame: no sustained response to CCh or exclusively ER Ca^{2+} mobilization from stores (no response), oscillations that return to basal levels after each release event (baseline oscillations) (Figure 15A), oscillations that returned to an elevated plateau above basal level (oscillations + elevated plateau) (Figure 15B) and sustained elevation above basal level without oscillations (elevated plateau) (Figure 15C).

When stimulated with 5 μM CCh (Figure 15D), 57% of control cells did not display a response, and the distribution of responses with baseline oscillations, oscillations + elevated plateau and elevated plateau were 29%, 4%, and 10% respectively. TRICA expression shifted the distribution pattern with 5 μM CCh to the lower response categories, with 69% non-responders, and no cells displaying an elevated plateau of $[Ca^{2+}]_i$. Upon stimulation with 100 μM CCh (Figure 15E), the majority of control cells (56%) displayed an elevated plateau and only 16% showed baseline oscillations. TRICA expression reduced the fraction of cells showing elevated plateau responses to 31% while increasing the proportion cells with baseline oscillations to 27%. Sustained elevation or oscillations in agonist-stimulated HEK293 cells are driven by SOCE (Ong et al., 2015, Bird et al., 2009). Thus, the TRICA-induced changes are likely based on the reduction in SOCE.

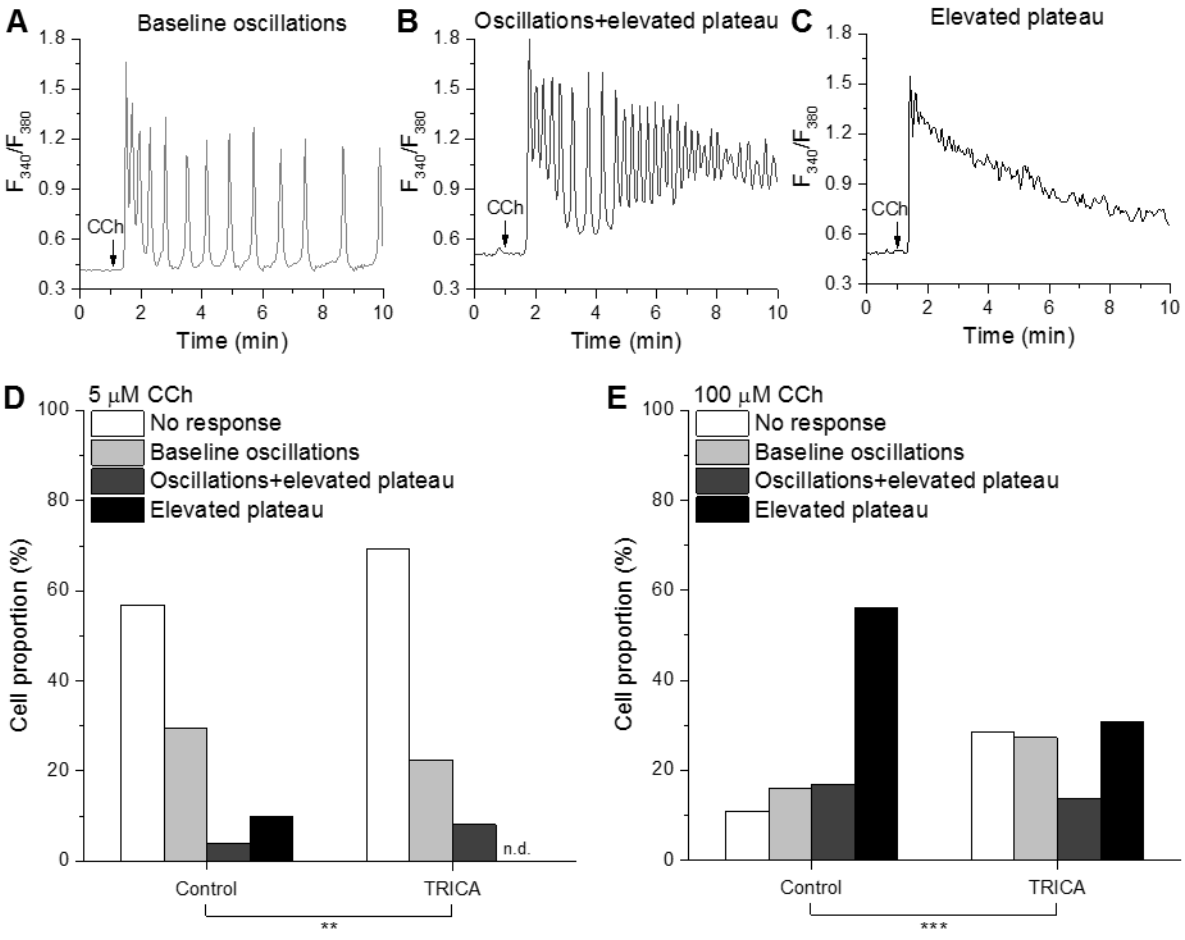

Figure 15. TRICA dampens SOCE-associated $[Ca^{2+}]_i$ responses to low and high stimuli levels.

(A-C) Representative traces showing various indicated $[Ca^{2+}]_i$ responses in cells stimulated with 5 or 100 μM CCh (arrow). **(D, E)** Bars show proportion (%) of cell population displaying various patterns of $[Ca^{2+}]_i$ response to (D) 5 μM and (E) 100 μM CCh. Overall patterns in TRICA (+) cells (n=169) were significantly different from that in controls (n=137) at 5 and 100 μM CCh; **p<0.01,***p<0.001; χ^2 test.

3.5 TRICA delays cyclic Ca^{2+} refilling upon store depletion

SOCE modulation by TRICA was further confirmed in experiments monitoring the time course of $[Ca^{2+}]_{ER}$ during store depletion by caffeine and its subsequent refilling by elevation of $[Ca^{2+}]_o$ from nominally free to 1 mM in HEK293_RyR2 cells (Figure 16A). Similar to spontaneous oscillations observed earlier (Figure 11), the time course of ER Ca^{2+} refilling after a caffeine-induced ER discharge was significantly slowed, and luminal Ca^{2+} oscillations induced by $[Ca^{2+}]_o$ were delayed in onset and had reduced frequency. TRICA expression prolonged the time to complete ER refilling by 0.61 ± 0.06 min (Figure 16B), reducing the rate of refilling by 26%, compared to controls (Figure 16C). Likewise, in the presence of 3 µM BTP2, ER refilling was occluded following store depletion by caffeine (Figure 16A), as a result of the elimination of SOCE. Hence TRICA impacts both ER Ca^{2+} store refilling and generation of cytosolic Ca^{2+} oscillations. However, TRICA did not enhance ER Ca^{2+} release induced by caffeine (Figure 16D). In aggregate, these findings strongly suggest TRICA as a potential regulator of SOCE during oscillatory Ca^{2+} signaling.

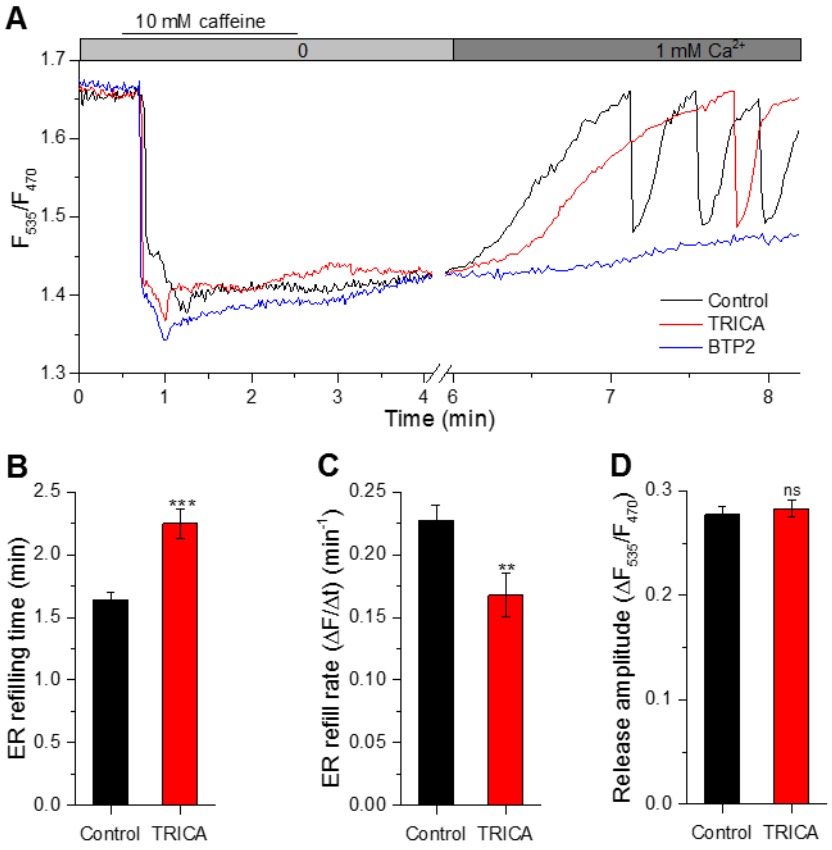

Figure 16. TRICA delays cyclic Ca^{2+} refilling upon store depletion.

(A) $[Ca^{2+}]_{ER}$-sensitive D1ER traces representing ER Ca^{2+} depletion with 10 mM caffeine, followed by ER refilling upon 1 mM $[Ca^{2+}]_o$ addition in mCherry-ER3 (control, black) or TRICA-mCherry (TRICA, red) transfected HEK293_RyR2 cell or diminished refilling in 3 μM BTP2-incubated control cell (BTP2, blue) . Bars show mean ± SEM values for **(B)** ER refilling time, **(C)** ER refill rate, and **(D)** ER Ca^{2+} release peak amplitude in TRICA (+) cells (n=45) vs. controls (n=51); **p<0.01, ***p<0.001, ns (non-significant).

3.6 TRICA inhibits Orai1-mediated recombinant I_{CRAC} upon store depletion

To examine the impact of TRICA on SOCE directly, we measured the SOCE-associated, Ca^{2+}-selective CRAC currents (I_{CRAC}). Since I_{CRAC} generated by endogenous STIM1/Orai1 is minute in HEK293 cells, YFP-STIM1 and Orai1-CFP were co-expressed along with mCherry-ER3 (control) or TRICA-mCherry, and I_{CRAC} was measured using whole cell patch clamp technique (Figure 17A). Figure 17B illustrates a representative current-voltage (I-V) relationship of the currents at 10 mM Ca^{2+}. While there was no change in reversal potential, the magnitude of the inward current was significantly reduced (current density at -80 mV = -8.30±0.87 pA/pF in TRICA-expressing cells vs. -11.82±0.99 pA/pF in controls) (Figure 17C). TRICA also slowed the rate of I_{CRAC} activation by 30%, though not significant (Figure 17D).

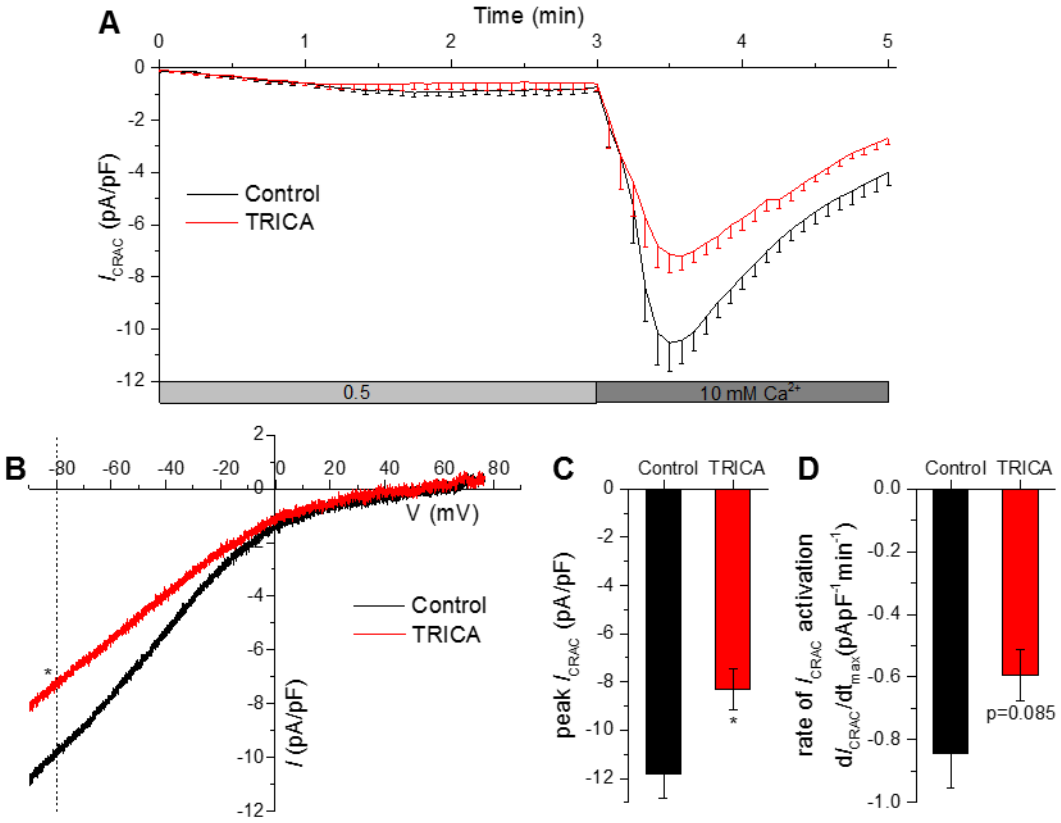

Figure 17. TRICA inhibits Orai1-mediated recombinant I_{CRAC} upon store depletion.

(A) Time course (mean - SEM) of I_{CRAC} at -80 mV in whole-cell voltage-clamp, mediated by YFP-STIM1 + Orai1-CFP, co-expressed along with mCherry-ER3 (control, n=13) or TRICA-mCherry (TRICA, n=11) in HEK293 cells. Current activation was mediated by ER store depletion with 10 mM EGTA in the patch pipette solution and stepwise current increment was recorded at 0.5 and 10 mM Ca^{2+} in the bath solution. **(B)** Traces show representative peak I-V relationship in control and TRICA groups at 10 mM Ca^{2+}. **(C, D)** Bars show mean ± SEM values for (C) peak I_{CRAC} and (D) maximum rate of I_{CRAC} activation in 10 mM Ca^{2+} at -80 mV, *p<0.05.

3.7 TRICA co-clusters with STIM1 at ER-PM junctions upon store depletion

To gain further insight into the mechanism underlying reduced SOCE and I_{CRAC}, we characterized the impact of TRICA on the initial molecular process of SOCE activation, where dissociation of luminal Ca^{2+} from the EF-hand motifs in STIM1 leads to its oligomerization and translocation into discrete puncta within ER-PM junctions (Roos et al., 2005, Wu et al., 2006, Liou et al., 2007). As observed by TIRF microscopy, the formation of YFP-STIM1 puncta in HEK293 cells was comparable to that in TRICA-expressing cells, indicating that the initial process of STIM1 activation was unaffected by TRICA. Both YFP-STIM1 and TRICA-mCherry, when co-expressed, localized in ER membranes forming network-like structures at basal, unstimulated conditions (Figure 18A, top). Interestingly, TRICA-mCherry dynamically translocated to co-cluster with YFP-STIM1 within puncta upon ER Ca^{2+} store depletion (Figure 18A, bottom), as evident from the overlay and line-scan analysis (Figure 18B). Notably, clustering of TRICA-mCherry required co-expressed STIM1, as clustering was absent when TRICA was expressed alone (Figure 18C). In contrast, YFP-STIM1 did not require co-expression of TRICA to form puncta upon ER Ca^{2+} store depletion (Figure 18D).

Co-immunoprecipitation experiments (Figure 18E) confirmed the physical interaction between TRICA and STIM1. TRICA-mCherry immunoprecipitated with myc-STIM1 even at basal, unstimulated conditions. Interestingly, no increase in TRICA-STIM1 association was observed upon store depletion, suggesting that TRICA-STIM1 interaction was independent of the Ca^{2+} filling state of the ER stores.

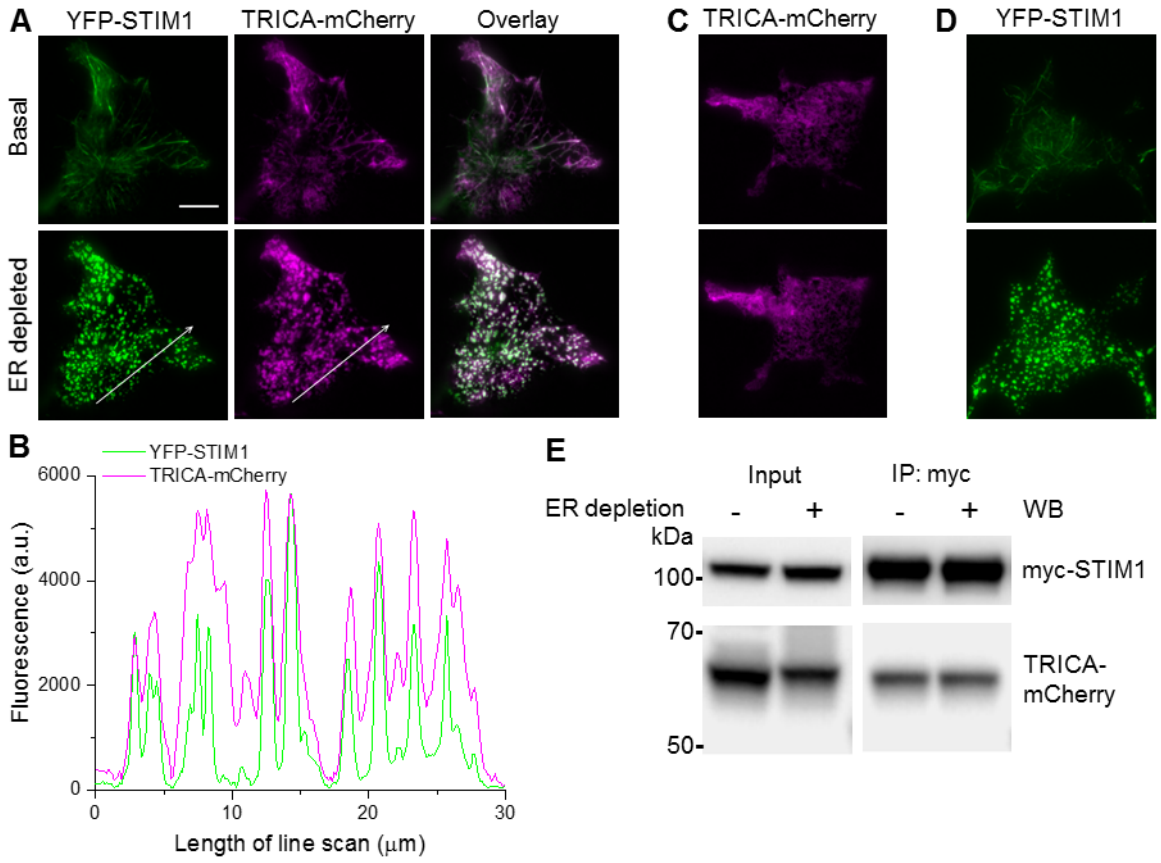

Figure 18. TRICA co-clusters with STIM1 at ER-PM junctions upon store depletion.

(A) Representative TIRFM images of basal (top) and ER depleted (100 μM CCh + 30 μM BHQ) (bottom) HEK293 cell expressing YFP-STIM1 (left, green) and TRICA-mCherry (middle, magenta) with an overlay (right) of both proteins. **(B)** Line scans of YFP-STIM1 and TRICA-mCherry in ER depleted cell shown in (A). **(C, D)** Representative TIRFM images of basal (top) and ER depleted (bottom) HEK293 cell expressing TRICA-mCherry and YFP-STIM1 separately. Scale bar=10 μm. **(E)** Representative co-immunoprecipitation of TRICA-mCherry with myc-STIM1, co-expressed in HEK293 cells. Lysates were obtained from basal (-) and ER depleted (+) (100 μM CCh + 30 μM BHQ) cells, n=3 independent experiments.

The data from co-immunoprecipitation was further confirmed by the co-expression of TRICA-mCherry with the EF-hand mutant of STIM1 (YFP-STIM1-D76A). This STIM1 mutant is constitutively active, thereby forming pre-clusters under basal, unstimulated conditions, and displays no significant increase in puncta aggregation following ER Ca^{2+} depletion (Liou et al., 2005). TRICA clustered with YFP-STIM1-D76A independently of ER Ca^{2+} depletion when co-expressed in the same cell, evident from the overlay and line-scan analysis (Figure 19). Thus, TRICA-STIM1 interaction appears to be independent of ER Ca^{2+} depletion. Considering a physical interaction between TRICA and STIM1 that

interferes and modulates spatiotemporal Ca^{2+} signaling via STIM1/Orai1, we next focused on a quantitative analysis of the underlying productive translocation and clustering processes.

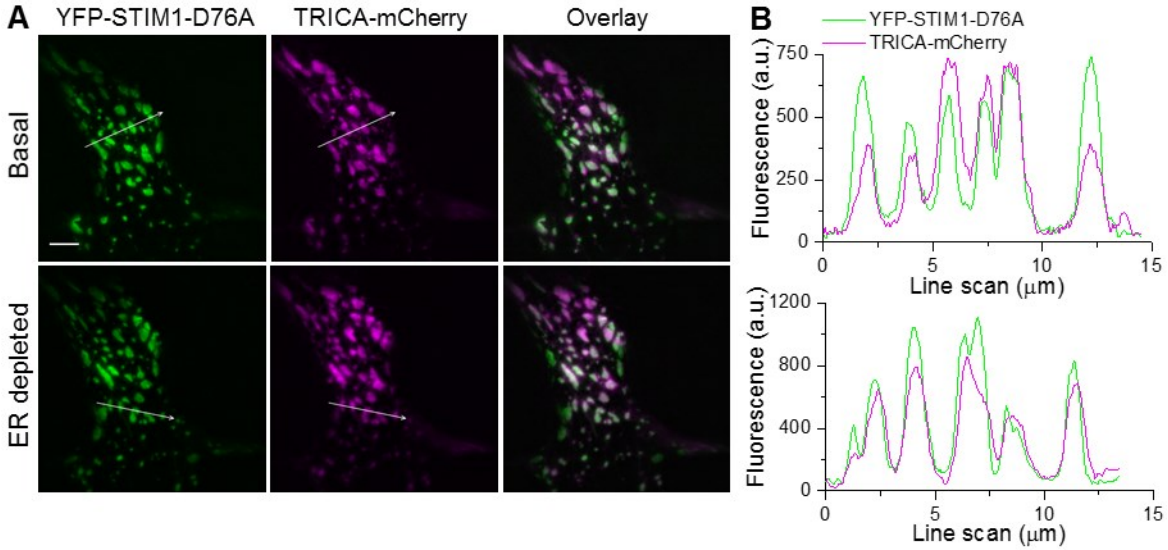

Figure 19. TRICA co-clusters with STIM1 EF-hand mutant independent of store depletion.
(A) Representative TIRFM images of basal (top) and ER depleted (100 μM CCh + 30 μM BHQ) (bottom) HEK293 cell expressing YFP-STIM1-D76A (left, green) and TRICA-mCherry (middle, magenta) with an overlay (right) of both proteins. Scale bar=5 μm, n=5 from 3 different experiments. **(B)** Line scans of YFP-STIM1-D76A and TRICA-mCherry in basal and ER depleted cell shown in (A).

3.8 TRICA affects kinetics and extent of STIM1-Orai1 puncta formation

SOCE depends on the assembly of STIM1/Orai1 complex within ER-PM junctions. Any impairment of the clustering of these proteins may hinder their interaction and suppress Orai1 channel activation and SOCE (Muik et al., 2009, Park et al., 2009, Yuan et al., 2009). Consequently, we analyzed the impact of TRICA on the clustering of STIM1 with Orai1 within ER-PM junctions. In HEK293 cells co-expressing Orai1-CFP and YFP-STIM1, together with mCherry-ER3 (Figure 20A, control) or TRICA-mCherry (Figure 20B, TRICA), the proteins clustered and formed discrete puncta upon ER Ca^{2+} depletion. The rate of Orai1 puncta assembly was significantly delayed in cells expressing TRICA (Figures 20C, 20E). Although TRICA similarly tended to delay STIM1 puncta formation, this effect was not statistically significant (Figure 20D, 20E). Besides, the average fluorescence intensity in Orai1 and STIM1 puncta of control and TRICA (+) cells was similar before and after ER Ca^{2+} depletion (Figure 20F). Moreover, the basal epifluorescence intensity of both proteins was unaffected by TRICA expression (Figure 20G).

Importantly, TRICA significantly reduced the colocalization of STIM1 and Orai1 within each puncta (Figure 21A). The overall size distribution of puncta for Orai1 (Figure 21B) and STIM1 (Figure 21C) was significantly altered by TRICA expression as compared to controls (***$p<0.001$; χ^2 test). TRICA cells displayed a higher fraction of puncta displaying the smallest size (0.04-0.2 μm) but reduced proportion of large clusters (0.4-1.4 μm) when compared to controls. Hence, average puncta size for both Orai1 and STIM1 was significantly reduced in TRICA-expressing cells (Figure 21D), indicating a reduced footprint for the STIM1/Orai1 puncta in the cell (Figure 21E). However, TRICA expression did not alter the number of puncta per membrane area (density) for both Orai1 and STIM1 (Figure 21F). Together, the data in figures 19, 20 and 21 indicate that TRICA interacts with STIM1 and is recruited by STIM1 to ER-PM junctions. Within the junctions, TRICA impedes clustering of STIM1 with Orai1 as well as their interaction.

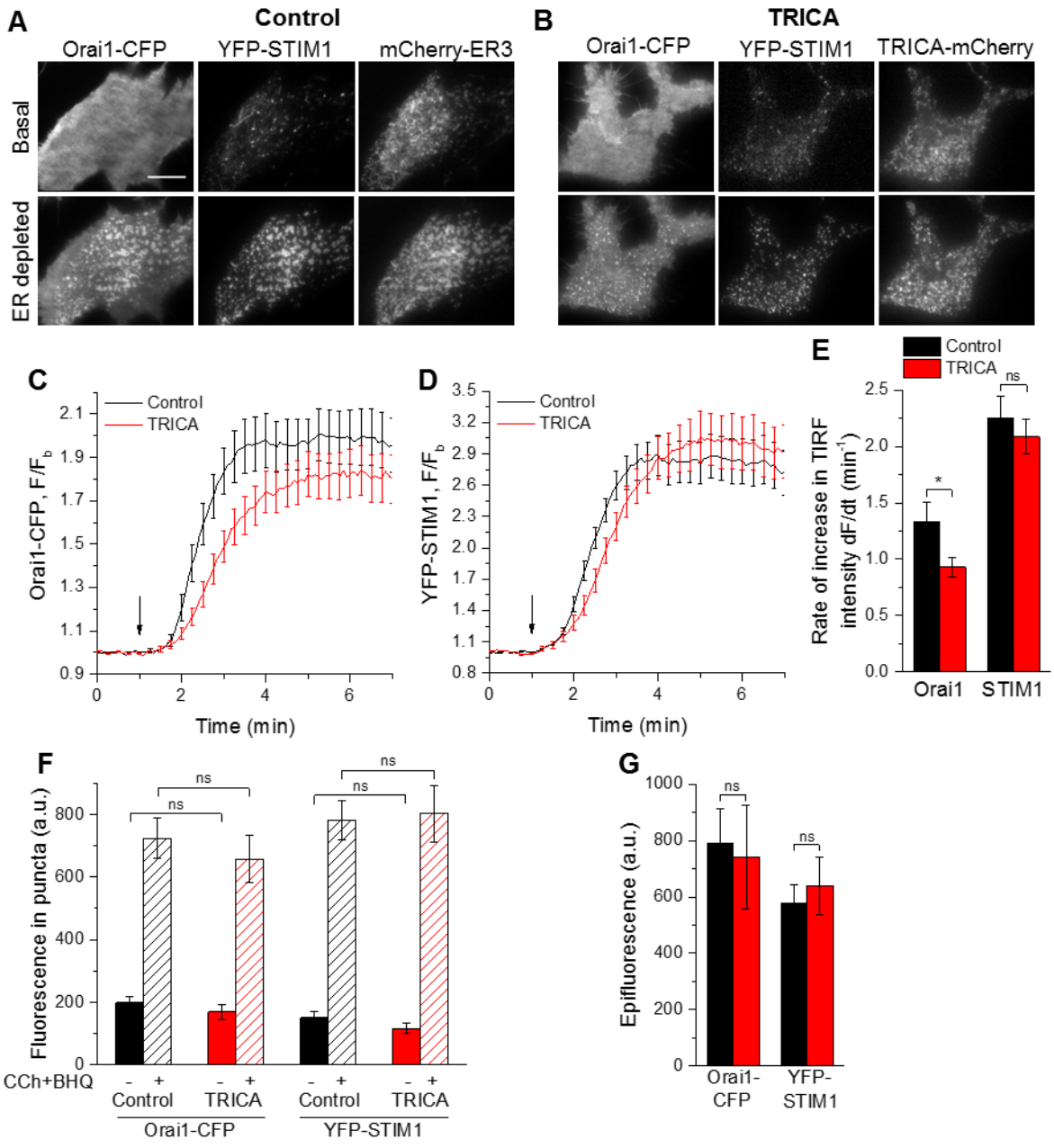

Figure 20. TRICA delays the rate of STIM1-Orai1 puncta formation upon store depletion.

(A, B) TIRFM images of basal (top) and ER depleted (100 μM CCh + 30 μM BHQ) (bottom) cell expressing Orai1-CFP (left) and YFP-STIM1 (middle) along with mCherry-ER3 (right) (A, control) or TRICA-mCherry (right) (B, TRICA). Scale bar=10 μm. **(C, D)** Traces show kinetics of Orai1-CFP and YFP-STIM1 TIRF intensity upon ER depletion (arrow) in TRICA (+) cells vs. controls (n=18 each). **(E)** Rate of increase in Orai1 and STIM1 TIRF intensity upon ER Ca^{2+} depletion shown in C, D. **(F)** Fluorescence in Orai1 and STIM1 puncta of control and TRICA (+) cells in the absence (-) and presence (+) of 100 μM CCh + 30 μM BHQ, repeated measures (mixed model) two-way ANOVA with Bonferroni post-tests. **(G)** Epifluorescence of Orai1-CFP and YFP-STIM1 in TRICA (+) cells vs. controls. *p<0.05, ns (non-significant); bars show mean ± SEM values.

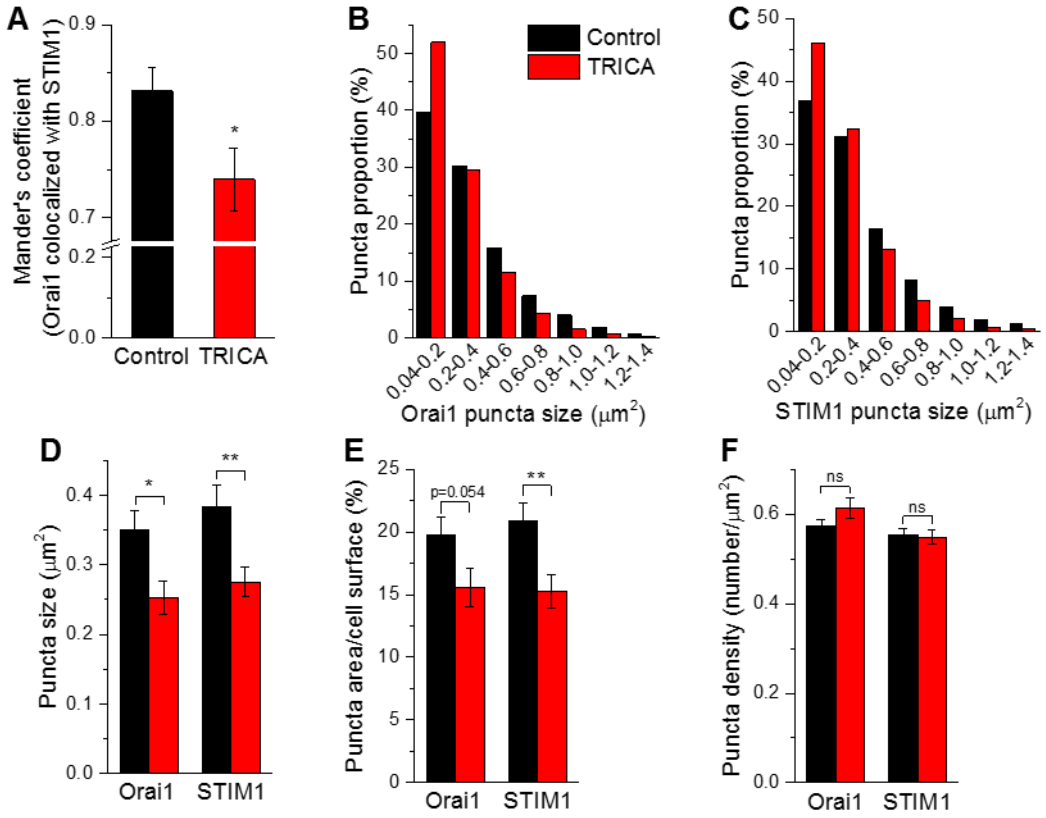

Figure 21. TRICA affects colocalization and size distribution of STIM1-Orai1 puncta upon store depletion, related to Figure 20.

(A) Mander's coefficient showing proportion of Orai1 colocalized with STIM1, **(B, C)** Proportion of puncta (%) of various sizes of (B) Orai1-CFP (number of puncta=4462 vs. 4836) and (C) YFP-STIM1 (number of puncta=4357 vs. 4519) in control and TRICA (+) cells. **(D)** Average puncta size distribution in TRICA cells was significantly different from that in controls (***p<0.001; χ^2 test). (D), **(E)** puncta area relative to cell surface area (%), and **(F)** puncta density of Orai1 and STIM1 in TRICA (+) cells vs. controls. *p<0.05, **p<0.01, ns (non-significant); mean ± SEM values are shown.

3.9 TRICA inhibits STIM1-Orai1 interaction upon store depletion

As gating of Orai1 channel is triggered by physical interaction of the channel with STIM1, we used FRET technique to assess the assembly of STIM1-CFP/YFP-Orai1 complex in response to ER Ca^{2+} store depletion (Figure 22A). Stimulation of cells with BHQ + CCh induced a fast and distinct increase of FRET in control and TRICA-expressing cells. Peak FRET increase was significantly diminished in cells expressing TRICA (by 32%) as compared to controls (Figure 22B). Interestingly, while a high FRET was maintained in control cells, FRET measured in TRICA-expressing cells declined markedly to about 50% within 10 min, despite the continued presence of BHQ. This finding suggested that TRICA profoundly affects the assembly of STIM1/Orai1 complex at ER-PM junctions by directly interfering with STIM1-Orai1 interaction. The decline in FRET suggests that STIM1/Orai1 interaction in TRICA-expressing cells might be less stable as compared to that in control cells.

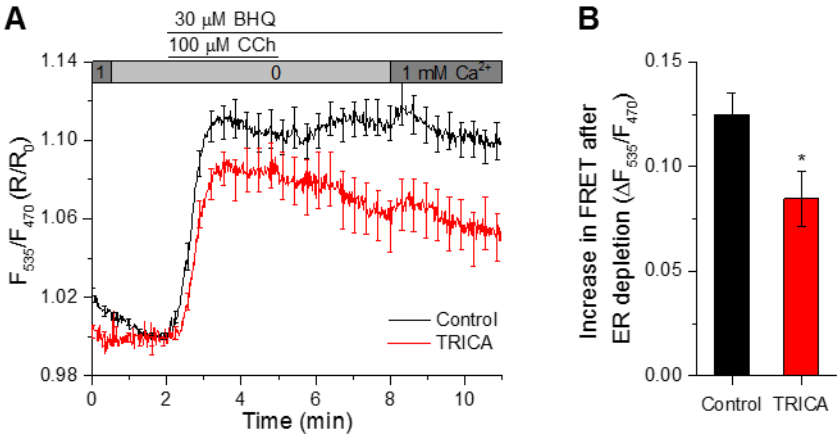

Figure 22. TRICA inhibits STIM1-Orai1 interaction upon store depletion.

(A) Traces show dynamic FRET between STIM1-CFP and YFP-Orai1 FRET co-transfected in HEK293 cells along with mCherry-ER3 (control, n=20) or TRICA-mCherry (TRICA, n=13). **(B)** Increase in STIM1-Orai1 FRET shown in (G) upon ER depletion with 100 µM CCh + 30 µM BHQ and SOCE in TRICA cells vs. controls. *p<0.05; mean ± SEM values are shown.

4. Discussion

Overall, our investigations demonstrate a novel function of TRICA in STIM1/Orai1-mediated SOCE pathway. As summarized in figure 23, we present multiple lines of evidence to demonstrate that TRICA channels interfere with the STIM1/Orai1 assembly and function: (i) TRICA is recruited by STIM1 to form puncta within the ER-PM junctions following Ca^{2+} store depletion, (ii) TRICA co-localizes with STIM1 and Orai1 puncta, (iii) TRICA interacts with STIM1, (iv) TRICA decreases STIM1/Orai1 interaction, and (v) TRICA attenuates I_{CRAC} and SOCE. Together, our findings suggest that TRICA is a negative regulator of SOCE that shapes cytosolic Ca^{2+} oscillations by modulating STIM1/Orai1 assembly and ER Ca^{2+} recycling.

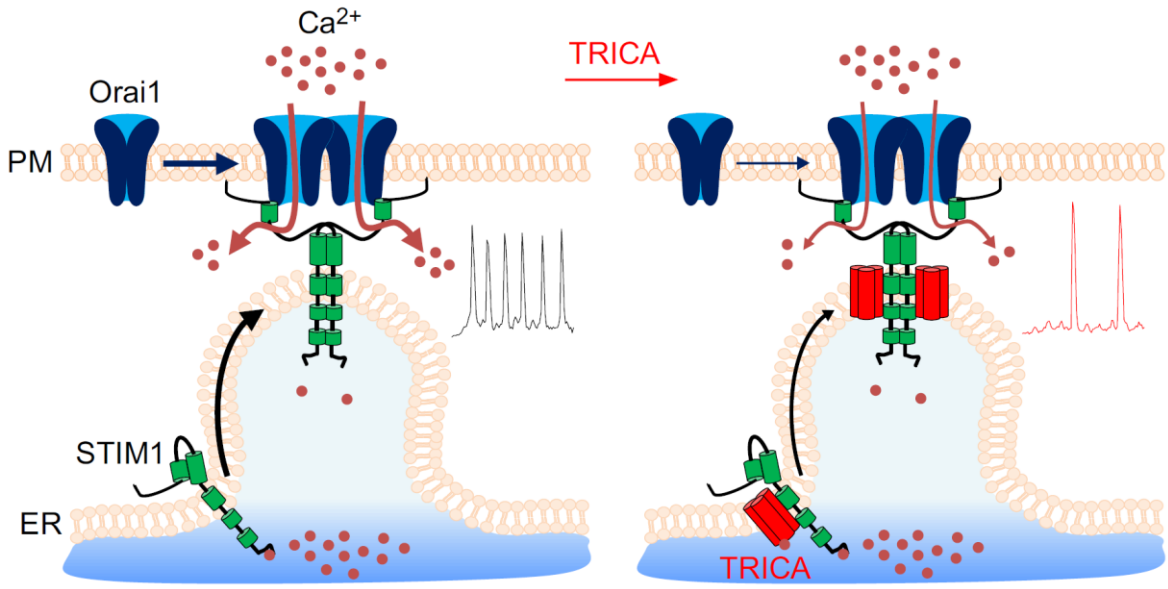

Figure 23. Schematic diagram illustrating the role of TRICA in modulating oscillatory Ca^{2+} signals by interaction with STIM1/Orai1 complexes.
Left: Upon ER Ca^{2+} depletion via RyR/IP_3R, STIM1 loses bound Ca^{2+} from its EF-hand, oligomerizes and translocates into clusters at ER-PM junctions and attaches to PM lipids via polybasic tail. STIM1 then recruits Orai1 channels into the clusters, activates the Ca^{2+} selective pore for subsequent Ca^{2+} entry into the cells to sustain RyR/IP_3R-triggered Ca^{2+} oscillations. **Right:** Overexpressed TRICA channels translocate along with STIM1 to ER-PM junctions where they delay Orai1 recruitment and coupling to STIM1 clusters, thereby limiting Ca^{2+} entry-sustained oscillations.

To our knowledge, this is the first report of TRICA interference with STIM1/Orai1 assembly and function. Our data further reveal that the recruitment of

TRICA into ER-PM junctions is triggered by ER Ca^{2+} depletion but is mediated by its interaction with STIM1 rather than its own ER Ca^{2+} sensing function (Wang et al., 2019). STIM1-D76A, a STIM1 mutant with disrupted luminal Ca^{2+} binding in its N-terminal EF-hand domain, displays constitutive clustering in ER-PM junctions (Liou et al., 2005). Pre-clustering of this STIM1 mutant is sufficient for promoting co-clustering of TRICA in ER-PM junctions, in the absence of store depletion. Of note, endogenous STIM1 per se appeared insufficient to produce significant clustering of overexpressed TRICA, implying that TRICA stoichiometry relative to STIM1 is critical for the extent of co-targeting into STIM1 clusters. In cells co-expressing Orai1 and STIM1, TRICA attenuates the assembly of STIM1 and Orai1 as evidenced by the reduction in the FRET signal that is generated due to an interaction between the two proteins. The decreased FRET, together with the changes in the pattern of clustering of Orai1/STIM1 can account for the decrease in SOCE. Importantly, the refilling of ER Ca^{2+} stores is attenuated by TRICA. Our findings provide strong evidence that this delay is due to disruption of STIM1/Orai1 assembly and consequent decrease in SOCE, which is required for refilling the intracellular Ca^{2+} stores. An additional, more direct, effect of TRICA on SERCA pump cannot be ruled out. Importantly, TRICA elicited the above effects without altering the expression of both endogenous and recombinant STIM1-Orai1. This is in line with the unaltered mRNA expression of endogenous STIM1 and Orai1 in mesenteric arteries and thoracic aorta of transgenic mice overexpressing TRICA (Tao et al., 2013).

TRICA has been previously shown to modulate Ca^{2+} handling in muscle cells by affecting RyR function (Yazawa et al., 2007, Zhao et al., 2010, Yamazaki et al., 2011). We utilized an established model of RyR2-dependent oscillatory Ca^{2+} signaling in HEK293_RyR2 cells to decipher the cellular role of TRICA, since it represents a well-defined cellular Ca^{2+} oscillator of relatively simple molecular composition and mimics the cardiac Ca^{2+} signalling phenotype along with pathophysiological significance for arrhythmia (Lakatta, 1992, Jiang et al., 2004). We demonstrate that these RyR2-mediated spontaneous Ca^{2+} oscillations are dependent on SOCE and can be completely abolished in the presence of the SOCE blocker, BTP2. Thus, by limiting SOCE, TRICA modulates SR/ER refilling and the frequency of the oscillations. Of note, TRICA-mediated suppression of

SOCE was not restricted to RyR2 expressing cells. Wild-type HEK293 cells lacking RyR2 also displayed clearly attenuated SOCE in presence of TRICA. This resulted in a shift in the Ca^{2+} signaling pattern from a sustained, elevated plateau to an oscillatory behavior in response to the physiological stimulation of PLC-IP_3 pathway, which might confer a protective effect against excess Ca^{2+} influx and overload in the cells.

In addition, the enhanced Ca^{2+} discharge amplitude during each oscillation is in line with the reported monovalent conductance generated by TRIC channels across the ER membrane, which has been proposed to facilitate Ca^{2+} efflux from the ER via K^+ counter flux (Yazawa et al., 2007, Yang et al., 2016). Instead, when both TRIC isoforms were knocked out in the embryonic cardiomyocytes, RyR2-triggered spontaneous Ca^{2+} oscillations were diminished as a consequence of compromised K^+ counterflux (Yazawa et al., 2007). The effects of TRICA on oscillation amplitude likely reflect crosstalk of the trimeric cation channel with RyR2-mediated Ca^{2+} mobilization since IP_3R-mediated Ca^{2+} release remained unaffected. Nevertheless, TRICA suppression of SOCE appears independent on the process of Ca^{2+} mobilization. Thus, TRICA represents a unique ER resident cation channel that governs the magnitude of ER Ca^{2+} mobilization process via its channel function and dictates the temporal features of the Ca^{2+} oscillations via interference with the STIM1/Orai1 coupling machinery within ER-PM junctions.

While the precise role of SOCE in muscle physiology is not fully understood, SOCE does play an important role in skeletal muscle physiology ranging development, differentiation, contractile function, and resistance against fatigue (Stiber et al., 2008, Darbellay et al., 2011, Li et al., 2012, Carrell et al., 2016, Boncompagni et al., 2017, Koenig et al., 2019). Skeletal muscle hypotonia and weakness are characteristics of STIM1- and Orai1-deficient patients and mice (Feske, 2010). While physiological SOCE is required for refilling SR Ca^{2+} stores and proper muscle development and function, excessive SOCE seems to be detrimental, leading to muscular dystrophy (Michelucci et al., 2018). STIM1 upregulation has also been associated with cardiac hypertrophy, hypertension, and arrhythmia, characterized by enhanced spontaneous Ca^{2+} transients and downstream transcription coupling, and decrease in its function has been

proposed to ameliorate these cardiac disorders (Voelkers et al., 2010, Hulot et al., 2011, Luo et al., 2012, Correll et al., 2015, Kassan et al., 2016, Parks et al., 2016, Benard et al., 2016). Thus, tight regulation of STIM1 function and SOCE is critical for maintaining proper muscle physiology based on oscillatory Ca^{2+} signals. The overloading of SR Ca^{2+} stores, aberrant ER-mitochondrial connections, and mitochondrial dysfunction associated with TRICA deficient muscle cells are indeed reminiscent of effects caused by increased STIM1 function. Thus, increased SOCE, in the absence of TRICA, can cause ER and mitochondrial Ca^{2+} overload. It is also of interest that another ER-resident protein, SARAF, when overexpressed, can mitigate the effect of STIM1 in cardiac hypertrophy and diastolic dysfunction (Dai et al., 2018). Interestingly, SARAF, like TRICA, is recruited to ER-PM junctions by STIM1 where it increases Ca^{2+}-dependent inactivation of Orai1 (Palty et al., 2012). Thus, two ER proteins negatively modulate STIM1/Orai1 function in muscle cells to limit SOCE and prevent SR Ca^{2+} overload. Further studies will be required to evaluate their individual effects on SOCE and the consequent physiological impact in muscles.

In summary, our findings suggest that TRICA-mediated regulation of SOCE can play a major role in regulating Ca^{2+} homeostasis in muscle cells. In addition, loss of TRICA, and a consequent gain of SOCE can disrupt Ca^{2+} handling resulting in long-term consequences and dysfunction. Indeed TRICA variants have been associated with hypertension in patients (Yamazaki et al., 2011). Since both TRICA and SOCE impact skeletal, cardiac as well as smooth muscle function, the TRICA-SOCE interaction might reflect a common mechanism to prevent SR Ca^{2+}-overload and dysfunction in these types of muscles. Therapies targeting SOCE could be beneficial in patients with TRICA defects.

5. Bibliography

Baba, Y., Hayashi, K., Fujii, Y., Mizushima, A., Watarai, H., Wakamori, M., Numaga, T., Mori, Y., Iino, M., Hikida, M. & Kurosaki, T. 2006. Coupling of STIM1 to store-operated Ca2+ entry through its constitutive and inducible movement in the endoplasmic reticulum. *Proc Natl Acad Sci U S A,* 103**,** 16704-9.

Benard, L., Oh, J. G., Cacheux, M., Lee, A., Nonnenmacher, M., Matasic, D. S., Kohlbrenner, E., Kho, C., Pavoine, C., Hajjar, R. J. & Hulot, J. S. 2016. Cardiac Stim1 Silencing Impairs Adaptive Hypertrophy and Promotes Heart Failure Through Inactivation of mTORC2/Akt Signaling. *Circulation,* 133**,** 1458-71; discussion 1471.

Berridge, M. J., Lipp, P. & Bootman, M. D. 2000. The versatility and universality of calcium signalling. *Nat Rev Mol Cell Biol,* 1**,** 11-21.

Bird, G. S., Hwang, S. Y., Smyth, J. T., Fukushima, M., Boyles, R. R. & Putney, J. W., Jr. 2009. STIM1 is a calcium sensor specialized for digital signaling. *Curr Biol,* 19**,** 1724-9.

Boie, S., Chen, J., Sanderson, M. J. & Sneyd, J. 2017. The relative contributions of store-operated and voltage-gated Ca(2+) channels to the control of Ca(2+) oscillations in airway smooth muscle. *J Physiol,* 595**,** 3129-3141.

Boncompagni, S., Michelucci, A., Pietrangelo, L., Dirksen, R. T. & Protasi, F. 2017. Exercise-dependent formation of new junctions that promote STIM1-Orai1 assembly in skeletal muscle. *Sci Rep,* 7**,** 14286.

Brandman, O., Liou, J., Park, W. S. & Meyer, T. 2007. STIM2 is a feedback regulator that stabilizes basal cytosolic and endoplasmic reticulum Ca2+ levels. *Cell,* 131**,** 1327-39.

Cai, X., Zhou, Y., Nwokonko, R. M., Loktionova, N. A., Wang, X., Xin, P., Trebak, M., Wang, Y. & Gill, D. L. 2016. The Orai1 Store-operated Calcium Channel Functions as a Hexamer. *J Biol Chem,* 291**,** 25764-25775.

Calloway, N., Holowka, D. & Baird, B. 2010. A basic sequence in STIM1 promotes Ca2+ influx by interacting with the C-terminal acidic coiled coil of Orai1. *Biochemistry,* 49**,** 1067-71.

Calloway, N., Vig, M., Kinet, J. P., Holowka, D. & Baird, B. 2009. Molecular clustering of STIM1 with Orai1/CRACM1 at the plasma membrane depends dynamically on depletion of Ca2+ stores and on electrostatic interactions. *Mol Biol Cell,* 20**,** 389-99.

Carrell, E. M., Coppola, A. R., Mcbride, H. J. & Dirksen, R. T. 2016. Orai1 enhances muscle endurance by promoting fatigue-resistant type I fiber content but not through acute store-operated Ca2+ entry. *FASEB J,* 30**,** 4109-4119.

Carreras-Sureda, A., Cantero-Recasens, G., Rubio-Moscardo, F., Kiefer, K., Peinelt, C., Niemeyer, B. A., Valverde, M. A. & Vicente, R. 2013. ORMDL3 modulates store-operated calcium entry and lymphocyte activation. *Hum Mol Genet,* 22**,** 519-30.

Cheng, K. T., Liu, X., Ong, H. L., Swaim, W. & Ambudkar, I. S. 2011. Local Ca(2)+ entry via Orai1 regulates plasma membrane recruitment of TRPC1 and controls cytosolic Ca(2)+ signals required for specific cell functions. *PLoS Biol,* 9**,** e1001025.

Collins, H. E., He, L., Zou, L., Qu, J., Zhou, L., Litovsky, S. H., Yang, Q., Young, M. E., Marchase, R. B. & Chatham, J. C. 2014. Stromal interaction molecule 1 is essential for normal cardiac homeostasis through modulation of ER and mitochondrial function. *Am J Physiol Heart Circ Physiol,* 306**,** H1231-9.

Correll, R. N., Goonasekera, S. A., Van Berlo, J. H., Burr, A. R., Accornero, F., Zhang, H., Makarewich, C. A., York, A. J., Sargent, M. A., Chen, X., Houser, S. R. & Molkentin, J. D. 2015. STIM1 elevation in the heart results in aberrant Ca(2)(+) handling and cardiomyopathy. *J Mol Cell Cardiol,* 87**,** 38-47.

Covington, E. D., Wu, M. M. & Lewis, R. S. 2010. Essential role for the CRAC activation domain in store-dependent oligomerization of STIM1. *Mol Biol Cell,* 21**,** 1897-907.

Dai, F., Zhang, Y., Wang, Q., Li, Yang, Y., Ma, S. & Yang, D. 2018. Overexpression of SARAF Ameliorates Pressure Overload-Induced Cardiac Hypertrophy Through Suppressing STIM1-Orai1 in Mice. *Cell Physiol Biochem,* 47**,** 817-826.

Darbellay, B., Arnaudeau, S., Bader, C. R., Konig, S. & Bernheim, L. 2011. STIM1L is a new actin-binding splice variant involved in fast repetitive Ca2+ release. *J Cell Biol,* 194**,** 335-46.

Derler, I., Fahrner, M., Muik, M., Lackner, B., Schindl, R., Groschner, K. & Romanin, C. 2009. A Ca2(+)release-activated Ca2(+) (CRAC) modulatory domain (CMD) within STIM1 mediates fast Ca2(+)-dependent inactivation of ORAI1 channels. *J Biol Chem,* 284**,** 24933-8.

Derler, I., Plenk, P., Fahrner, M., Muik, M., Jardin, I., Schindl, R., Gruber, H. J., Groschner, K. & Romanin, C. 2013. The extended transmembrane Orai1 N-terminal (ETON) region combines binding interface and gate for Orai1 activation by STIM1. *J Biol Chem,* 288**,** 29025-34.

Di Capite, J., Ng, S. W. & Parekh, A. B. 2009. Decoding of cytoplasmic Ca(2+) oscillations through the spatial signature drives gene expression. *Curr Biol,* 19**,** 853-8.

Di Giuro, C. M. L., Shrestha, N., Malli, R., Groschner, K., Van Breemen, C. & Fameli, N. 2017. Na (+)/Ca(2+) exchangers and Orai channels jointly refill endoplasmic reticulum (ER) Ca(2+) via ER nanojunctions in vascular endothelial cells. *Pflugers Arch,* 469**,** 1287-1299.

Dolmetsch, R. E., Lewis, R. S., Goodnow, C. C. & Healy, J. I. 1997. Differential activation of transcription factors induced by Ca2+ response amplitude and duration. *Nature,* 386**,** 855-8.

Dolmetsch, R. E., Xu, K. & Lewis, R. S. 1998. Calcium oscillations increase the efficiency and specificity of gene expression. *Nature,* 392**,** 933-6.

Dupont, G., Combettes, L., Bird, G. S. & Putney, J. W. 2011. Calcium oscillations. *Cold Spring Harb Perspect Biol,* 3.

El-Ajouz, S., Venturi, E., Witschas, K., Beech, M., Wilson, A. D., Lindsay, C., Eberhardt, D., O'brien, F., Iida, T., Nishi, M., Takeshima, H. & Sitsapesan, R. 2017. Dampened activity of ryanodine receptor channels in mutant skeletal muscle lacking TRIC-A. *J Physiol,* 595**,** 4769-4784.

Fahrner, M., Muik, M., Schindl, R., Butorac, C., Stathopulos, P., Zheng, L., Jardin, I., Ikura, M. & Romanin, C. 2014. A coiled-coil clamp controls both conformation and clustering of stromal interaction molecule 1 (STIM1). *J Biol Chem,* 289**,** 33231-44.

Feng, J. M., Hu, Y. K., Xie, L. H., Colwell, C. S., Shao, X. M., Sun, X. P., Chen, B., Tang, H. & Campagnoni, A. T. 2006. Golli protein negatively regulates store depletion-induced calcium influx in T cells. *Immunity,* 24**,** 717-27.

Feske, S. 2010. CRAC channelopathies. *Pflugers Arch,* 460**,** 417-35.

Feske, S., Gwack, Y., Prakriya, M., Srikanth, S., Puppel, S. H., Tanasa, B., Hogan, P. G., Lewis, R. S., Daly, M. & Rao, A. 2006. A mutation in Orai1 causes immune deficiency by abrogating CRAC channel function. *Nature,* 441**,** 179-85.

Frischauf, I., Zayats, V., Deix, M., Hochreiter, A., Jardin, I., Muik, M., Lackner, B., Svobodova, B., Pammer, T., Litvinukova, M., Sridhar, A. A., Derler, I., Bogeski, I., Romanin, C., Ettrich, R. H. & Schindl, R. 2015. A calcium-accumulating region, CAR, in the channel Orai1 enhances Ca(2+) permeation and SOCE-induced gene transcription. *Sci Signal,* 8**,** ra131.

Giachini, F. R., Chiao, C. W., Carneiro, F. S., Lima, V. V., Carneiro, Z. N., Dorrance, A. M., Tostes, R. C. & Webb, R. C. 2009. Increased activation of stromal interaction molecule-1/Orai-1 in aorta from hypertensive rats: a novel insight into vascular dysfunction. *Hypertension,* 53**,** 409-16.

Grigoriev, I., Gouveia, S. M., Van Der Vaart, B., Demmers, J., Smyth, J. T., Honnappa, S., Splinter, D., Steinmetz, M. O., Putney, J. W., Jr., Hoogenraad, C. C. & Akhmanova, A. 2008. STIM1 is a MT-plus-end-tracking protein involved in remodeling of the ER. *Curr Biol,* 18**,** 177-82.

Groschner, K., Shrestha, N. & Fameli, N. 2017. Cardiovascular and Hemostatic Disorders: SOCE in Cardiovascular Cells: Emerging Targets for Therapeutic Intervention. *Adv Exp Med Biol,* 993**,** 473-503.

Groschner, K., Shrestha, N. & Fameli, N. 2018. Non-Orai Partners of STIM Proteins: Role in ER-PM Communication and Ca(2+) Signaling. *In:* KOZAK, J. A. & PUTNEY, J. W., JR. (eds.) *Calcium Entry Channels in Non-Excitable Cells.* Boca Raton (FL).

Gudlur, A., Quintana, A., Zhou, Y., Hirve, N., Mahapatra, S. & Hogan, P. G. 2014. STIM1 triggers a gating rearrangement at the extracellular mouth of the ORAI1 channel. *Nat Commun,* 5**,** 5164.

Guo, T., Nani, A., Shonts, S., Perryman, M., Chen, H., Shannon, T., Gillespie, D. & Fill, M. 2013. Sarcoplasmic reticulum K(+) (TRIC) channel does not carry essential countercurrent during Ca(2+) release. *Biophys J,* 105**,** 1151-60.

Horton, J. S., Buckley, C. L., Alvarez, E. M., Schorlemmer, A. & Stokes, A. J. 2014. The calcium release-activated calcium channel Orai1 represents a crucial component in hypertrophic compensation and the development of dilated cardiomyopathy. *Channels (Austin),* 8**,** 35-48.

Hoth, M. & Penner, R. 1992. Depletion of intracellular calcium stores activates a calcium current in mast cells. *Nature,* 355**,** 353-6.

Hou, X., Burstein, S. R. & Long, S. B. 2018. Structures reveal opening of the store-operated calcium channel Orai. *Elife,* 7.

Hou, X., Pedi, L., Diver, M. M. & Long, S. B. 2012. Crystal structure of the calcium release-activated calcium channel Orai. *Science,* 338**,** 1308-13.

Huang, G. N., Zeng, W., Kim, J. Y., Yuan, J. P., Han, L., Muallem, S. & Worley, P. F. 2006. STIM1 carboxyl-terminus activates native SOC, I(crac) and TRPC1 channels. *Nat Cell Biol,* 8**,** 1003-10.

Hulot, J. S., Fauconnier, J., Ramanujam, D., Chaanine, A., Aubart, F., Sassi, Y., Merkle, S., Cazorla, O., Ouille, A., Dupuis, M., Hadri, L., Jeong, D., Muhlstedt, S., Schmitt, J., Braun, A., Benard, L., Saliba, Y., Laggerbauer, B., Nieswandt, B., Lacampagne, A., Hajjar, R. J., Lompre, A. M. & Engelhardt, S. 2011. Critical role for stromal interaction molecule 1 in cardiac hypertrophy. *Circulation,* 124**,** 796-805.

Hunton, D. L., Lucchesi, P. A., Pang, Y., Cheng, X., Dell'italia, L. J. & Marchase, R. B. 2002. Capacitative calcium entry contributes to nuclear factor of activated T-cells nuclear translocation and hypertrophy in cardiomyocytes. *J Biol Chem,* 277**,** 14266-73.

Hunton, D. L., Zou, L., Pang, Y. & Marchase, R. B. 2004. Adult rat cardiomyocytes exhibit capacitative calcium entry. *Am J Physiol Heart Circ Physiol,* 286**,** H1124-32.

Jiang, D., Xiao, B., Yang, D., Wang, R., Choi, P., Zhang, L., Cheng, H. & Chen, S. R. 2004. RyR2 mutations linked to ventricular tachycardia and sudden death reduce the threshold for store-overload-induced Ca2+ release (SOICR). *Proc Natl Acad Sci U S A,* 101**,** 13062-7.

Jing, J., He, L., Sun, A., Quintana, A., Ding, Y., Ma, G., Tan, P., Liang, X., Zheng, X., Chen, L., Shi, X., Zhang, S. L., Zhong, L., Huang, Y., Dong, M. Q., Walker, C. L., Hogan, P. G., Wang, Y. & Zhou, Y. 2015. Proteomic mapping of ER-PM junctions identifies STIMATE as a regulator of Ca(2)(+) influx. *Nat Cell Biol,* 17**,** 1339-47.

Kar, P., Bakowski, D., Di Capite, J., Nelson, C. & Parekh, A. B. 2012. Different agonists recruit different stromal interaction molecule proteins to support cytoplasmic Ca2+ oscillations and gene expression. *Proc Natl Acad Sci U S A,* 109**,** 6969-74.

Kar, P., Nelson, C. & Parekh, A. B. 2011. Selective activation of the transcription factor NFAT1 by calcium microdomains near Ca2+ release-activated Ca2+ (CRAC) channels. *J Biol Chem,* 286**,** 14795-803.

Kassan, M., Ait-Aissa, K., Radwan, E., Mali, V., Haddox, S., Gabani, M., Zhang, W., Belmadani, S., Irani, K., Trebak, M. & Matrougui, K. 2016. Essential Role of Smooth Muscle STIM1 in Hypertension and Cardiovascular Dysfunction. *Arterioscler Thromb Vasc Biol,* 36**,** 1900-9.

Koenig, X., Choi, R. H., Schicker, K., Singh, D. P., Hilber, K. & Launikonis, B. S. 2019. Mechanistic insights into store-operated Ca(2+) entry during excitation-contraction coupling in skeletal muscle. *Biochim Biophys Acta Mol Cell Res,* 1866**,** 1239-1248.

Korzeniowski, M. K., Manjarres, I. M., Varnai, P. & Balla, T. 2010. Activation of STIM1-Orai1 involves an intramolecular switching mechanism. *Sci Signal,* 3**,** ra82.

Korzeniowski, M. K., Popovic, M. A., Szentpetery, Z., Varnai, P., Stojilkovic, S. S. & Balla, T. 2009. Dependence of STIM1/Orai1-mediated calcium entry on plasma membrane phosphoinositides. *J Biol Chem,* 284**,** 21027-35.

Krapivinsky, G., Krapivinsky, L., Stotz, S. C., Manasian, Y. & Clapham, D. E. 2011. POST, partner of stromal interaction molecule 1 (STIM1), targets STIM1 to multiple transporters. *Proc Natl Acad Sci U S A,* 108**,** 19234-9.

Lakatta, E. G. 1992. Functional implications of spontaneous sarcoplasmic reticulum Ca2+ release in the heart. *Cardiovasc Res,* 26**,** 193-214.

Lee, K. P., Choi, S., Hong, J. H., Ahuja, M., Graham, S., Ma, R., So, I., Shin, D. M., Muallem, S. & Yuan, J. P. 2014. Molecular determinants mediating gating of Transient Receptor Potential Canonical (TRPC) channels by stromal interaction molecule 1 (STIM1). *J Biol Chem,* 289**,** 6372-82.

Lee, K. P., Yuan, J. P., Zeng, W., So, I., Worley, P. F. & Muallem, S. 2009. Molecular determinants of fast Ca2+-dependent inactivation and gating of the Orai channels. *Proc Natl Acad Sci U S A,* 106**,** 14687-92.

Lefkimmiatis, K., Srikanthan, M., Maiellaro, I., Moyer, M. P., Curci, S. & Hofer, A. M. 2009. Store-operated cyclic AMP signalling mediated by STIM1. *Nat Cell Biol,* 11**,** 433-42.

Li, T., Finch, E. A., Graham, V., Zhang, Z. S., Ding, J. D., Burch, J., Oh-Hora, M. & Rosenberg, P. 2012. STIM1-Ca(2+) signaling is required for the hypertrophic growth of skeletal muscle in mice. *Mol Cell Biol,* 32**,** 3009-17.

Li, Z., Lu, J., Xu, P., Xie, X., Chen, L. & Xu, T. 2007. Mapping the interacting domains of STIM1 and Orai1 in Ca2+ release-activated Ca2+ channel activation. *J Biol Chem,* 282**,** 29448-56.

Liou, J., Fivaz, M., Inoue, T. & Meyer, T. 2007. Live-cell imaging reveals sequential oligomerization and local plasma membrane targeting of stromal interaction molecule 1 after Ca2+ store depletion. *Proc Natl Acad Sci U S A,* 104**,** 9301-6.

Liou, J., Kim, M. L., Heo, W. D., Jones, J. T., Myers, J. W., Ferrell, J. E., Jr. & Meyer, T. 2005. STIM is a Ca2+ sensor essential for Ca2+-store-depletion-triggered Ca2+ influx. *Curr Biol,* 15**,** 1235-41.

Lis, A., Zierler, S., Peinelt, C., Fleig, A. & Penner, R. 2010. A single lysine in the N-terminal region of store-operated channels is critical for STIM1-mediated gating. *J Gen Physiol,* 136**,** 673-86.

Litjens, T., Harland, M. L., Roberts, M. L., Barritt, G. J. & Rychkov, G. Y. 2004. Fast Ca(2+)-dependent inactivation of the store-operated Ca2+ current (ISOC) in liver cells: a role for calmodulin. *J Physiol,* 558**,** 85-97.

Liu, B., Peel, S. E., Fox, J. & Hall, I. P. 2010. Reverse mode Na+/Ca2+ exchange mediated by STIM1 contributes to Ca2+ influx in airway smooth muscle following agonist stimulation. *Respir Res,* 11**,** 168.

Liu, J., Xin, L., Benson, V. L., Allen, D. G. & Ju, Y. K. 2015. Store-operated calcium entry and the localization of STIM1 and Orai1 proteins in isolated mouse sinoatrial node cells. *Front Physiol,* 6**,** 69.

Luik, R. M., Wu, M. M., Buchanan, J. & Lewis, R. S. 2006. The elementary unit of store-operated Ca2+ entry: local activation of CRAC channels by STIM1 at ER-plasma membrane junctions. *J Cell Biol,* 174**,** 815-25.

Luo, X., Hojayev, B., Jiang, N., Wang, Z. V., Tandan, S., Rakalin, A., Rothermel, B. A., Gillette, T. G. & Hill, J. A. 2012. STIM1-dependent store-operated Ca(2)(+) entry is required for pathological cardiac hypertrophy. *J Mol Cell Cardiol,* 52**,** 136-47.

Lyfenko, A. D. & Dirksen, R. T. 2008. Differential dependence of store-operated and excitation-coupled Ca2+ entry in skeletal muscle on STIM1 and Orai1. *J Physiol,* 586**,** 4815-24.

Ma, G., Wei, M., He, L., Liu, C., Wu, B., Zhang, S. L., Jing, J., Liang, X., Senes, A., Tan, P., Li, S., Sun, A., Bi, Y., Zhong, L., Si, H., Shen, Y., Li, M., Lee, M. S., Zhou, W., Wang, J., Wang, Y. & Zhou, Y. 2015. Inside-out Ca(2+) signalling prompted by STIM1 conformational switch. *Nat Commun,* 6**,** 7826.

Ma, J., Goryaynov, A. & Yang, W. 2016. Super-resolution 3D tomography of interactions and competition in the nuclear pore complex. *Nat Struct Mol Biol,* 23**,** 239-47.

Manjarres, I. M., Rodriguez-Garcia, A., Alonso, M. T. & Garcia-Sancho, J. 2010. The sarco/endoplasmic reticulum Ca(2+) ATPase (SERCA) is the third element in capacitative calcium entry. *Cell Calcium,* 47**,** 412-8.

Maruyama, Y., Ogura, T., Mio, K., Kato, K., Kaneko, T., Kiyonaka, S., Mori, Y. & Sato, C. 2009. Tetrameric Orai1 is a teardrop-shaped molecule with a long, tapered cytoplasmic domain. *J Biol Chem,* 284**,** 13676-85.

Mcnally, B. A., Somasundaram, A., Jairaman, A., Yamashita, M. & Prakriya, M. 2013. The C- and N-terminal STIM1 binding sites on Orai1 are required for both trapping and gating CRAC channels. *J Physiol,* 591**,** 2833-50.

Mcnally, B. A., Somasundaram, A., Yamashita, M. & Prakriya, M. 2012. Gated regulation of CRAC channel ion selectivity by STIM1. *Nature,* 482**,** 241-5.

Mcnally, B. A., Yamashita, M., Engh, A. & Prakriya, M. 2009. Structural determinants of ion permeation in CRAC channels. *Proc Natl Acad Sci U S A,* 106**,** 22516-21.

Michelucci, A., Garcia-Castaneda, M., Boncompagni, S. & Dirksen, R. T. 2018. Role of STIM1/ORAI1-mediated store-operated Ca(2+) entry in skeletal muscle physiology and disease. *Cell Calcium,* 76**,** 101-115.

Mignen, O., Thompson, J. L. & Shuttleworth, T. J. 2008. Orai1 subunit stoichiometry of the mammalian CRAC channel pore. *J Physiol,* 586**,** 419-25.

Muik, M., Fahrner, M., Derler, I., Schindl, R., Bergsmann, J., Frischauf, I., Groschner, K. & Romanin, C. 2009. A Cytosolic Homomerization and a Modulatory Domain within STIM1 C Terminus Determine Coupling to ORAI1 Channels. *J Biol Chem,* 284**,** 8421-6.

Muik, M., Fahrner, M., Schindl, R., Stathopulos, P., Frischauf, I., Derler, I., Plenk, P., Lackner, B., Groschner, K., Ikura, M. & Romanin, C. 2011. STIM1 couples to ORAI1 via an intramolecular transition into an extended conformation. *EMBO J,* 30**,** 1678-89.

Muik, M., Frischauf, I., Derler, I., Fahrner, M., Bergsmann, J., Eder, P., Schindl, R., Hesch, C., Polzinger, B., Fritsch, R., Kahr, H., Madl, J., Gruber, H., Groschner, K. & Romanin, C. 2008.

Dynamic coupling of the putative coiled-coil domain of ORAI1 with STIM1 mediates ORAI1 channel activation. *J Biol Chem,* 283**,** 8014-22.

Mullins, F. M., Park, C. Y., Dolmetsch, R. E. & Lewis, R. S. 2009. STIM1 and calmodulin interact with Orai1 to induce Ca2+-dependent inactivation of CRAC channels. *Proc Natl Acad Sci U S A,* 106**,** 15495-500.

Mullins, F. M., Yen, M. & Lewis, R. S. 2016. Orai1 pore residues control CRAC channel inactivation independently of calmodulin. *J Gen Physiol,* 147**,** 137-52.

Ong, H. L., De Souza, L. B., Zheng, C., Cheng, K. T., Liu, X., Goldsmith, C. M., Feske, S. & Ambudkar, I. S. 2015. STIM2 enhances receptor-stimulated Ca(2)(+) signaling by promoting recruitment of STIM1 to the endoplasmic reticulum-plasma membrane junctions. *Sci Signal,* 8**,** ra3.

Oritani, K. & Kincade, P. W. 1996. Identification of stromal cell products that interact with pre-B cells. *J Cell Biol,* 134**,** 771-82.

Palmer, A. E., Jin, C., Reed, J. C. & Tsien, R. Y. 2004. Bcl-2-mediated alterations in endoplasmic reticulum Ca2+ analyzed with an improved genetically encoded fluorescent sensor. *Proc Natl Acad Sci U S A,* 101**,** 17404-9.

Palty, R. & Isacoff, E. Y. 2016. Cooperative Binding of Stromal Interaction Molecule 1 (STIM1) to the N and C Termini of Calcium Release-activated Calcium Modulator 1 (Orai1). *J Biol Chem,* 291**,** 334-41.

Palty, R., Raveh, A., Kaminsky, I., Meller, R. & Reuveny, E. 2012. SARAF inactivates the store operated calcium entry machinery to prevent excess calcium refilling. *Cell,* 149**,** 425-38.

Palty, R., Stanley, C. & Isacoff, E. Y. 2015. Critical role for Orai1 C-terminal domain and TM4 in CRAC channel gating. *Cell Res,* 25**,** 963-80.

Park, C. Y., Hoover, P. J., Mullins, F. M., Bachhawat, P., Covington, E. D., Raunser, S., Walz, T., Garcia, K. C., Dolmetsch, R. E. & Lewis, R. S. 2009. STIM1 clusters and activates CRAC channels via direct binding of a cytosolic domain to Orai1. *Cell,* 136**,** 876-90.

Park, C. Y., Shcheglovitov, A. & Dolmetsch, R. 2010. The CRAC channel activator STIM1 binds and inhibits L-type voltage-gated calcium channels. *Science,* 330**,** 101-5.

Parks, C., Alam, M. A., Sullivan, R. & Mancarella, S. 2016. STIM1-dependent Ca(2+) microdomains are required for myofilament remodeling and signaling in the heart. *Sci Rep,* 6**,** 25372.

Peinelt, C., Vig, M., Koomoa, D. L., Beck, A., Nadler, M. J., Koblan-Huberson, M., Lis, A., Fleig, A., Penner, R. & Kinet, J. P. 2006. Amplification of CRAC current by STIM1 and CRACM1 (Orai1). *Nat Cell Biol,* 8**,** 771-3.

Penna, A., Demuro, A., Yeromin, A. V., Zhang, S. L., Safrina, O., Parker, I. & Cahalan, M. D. 2008. The CRAC channel consists of a tetramer formed by Stim-induced dimerization of Orai dimers. *Nature,* 456**,** 116-20.

Pitt, S. J., Park, K. H., Nishi, M., Urashima, T., Aoki, S., Yamazaki, D., Ma, J., Takeshima, H. & Sitsapesan, R. 2010. Charade of the SR K+-channel: two ion-channels, TRIC-A and TRIC-B, masquerade as a single K+-channel. *Biophys J,* 99**,** 417-26.

Pozo-Guisado, E., Campbell, D. G., Deak, M., Alvarez-Barrientos, A., Morrice, N. A., Alvarez, I. S., Alessi, D. R. & Martin-Romero, F. J. 2010. Phosphorylation of STIM1 at ERK1/2 target sites modulates store-operated calcium entry. *J Cell Sci,* 123**,** 3084-93.

Prakriya, M., Feske, S., Gwack, Y., Srikanth, S., Rao, A. & Hogan, P. G. 2006. Orai1 is an essential pore subunit of the CRAC channel. *Nature,* 443**,** 230-3.

Prakriya, M. & Lewis, R. S. 2015. Store-Operated Calcium Channels. *Physiol Rev,* 95**,** 1383-436.

Prins, D., Groenendyk, J., Touret, N. & Michalak, M. 2011. Modulation of STIM1 and capacitative Ca2+ entry by the endoplasmic reticulum luminal oxidoreductase ERp57. *EMBO Rep,* 12**,** 1182-8.

Putney, J. W., Jr. 1986. A model for receptor-regulated calcium entry. *Cell Calcium,* 7**,** 1-12.

Putney, J. W., Jr. 1990. Capacitative calcium entry revisited. *Cell Calcium,* 11**,** 611-24.

Ritchie, M. F., Samakai, E. & Soboloff, J. 2012. STIM1 is required for attenuation of PMCA-mediated Ca2+ clearance during T-cell activation. *EMBO J,* 31**,** 1123-33.

Roos, J., Digregorio, P. J., Yeromin, A. V., Ohlsen, K., Lioudyno, M., Zhang, S., Safrina, O., Kozak, J. A., Wagner, S. L., Cahalan, M. D., Velicelebi, G. & Stauderman, K. A. 2005. STIM1, an essential and conserved component of store-operated Ca2+ channel function. *J Cell Biol,* 169**,** 435-45.

Sampieri, A., Zepeda, A., Asanov, A. & Vaca, L. 2009. Visualizing the store-operated channel complex assembly in real time: identification of SERCA2 as a new member. *Cell Calcium,* 45**,** 439-46.

Seth, M., Li, T., Graham, V., Burch, J., Finch, E., Stiber, J. A. & Rosenberg, P. B. 2012. Dynamic regulation of sarcoplasmic reticulum Ca(2+) stores by stromal interaction molecule 1 and sarcolipin during muscle differentiation. *Dev Dyn,* 241**,** 639-47.

Sharma, S., Quintana, A., Findlay, G. M., Mettlen, M., Baust, B., Jain, M., Nilsson, R., Rao, A. & Hogan, P. G. 2013. An siRNA screen for NFAT activation identifies septins as coordinators of store-operated Ca2+ entry. *Nature,* 499**,** 238-42.

Shen, W. W., Frieden, M. & Demaurex, N. 2011. Local cytosolic Ca2+ elevations are required for stromal interaction molecule 1 (STIM1) de-oligomerization and termination of store-operated Ca2+ entry. *J Biol Chem,* 286**,** 36448-59.

Soboloff, J., Madesh, M. & Gill, D. L. 2011. Sensing cellular stress through STIM proteins. *Nat Chem Biol,* 7**,** 488-92.

Soboloff, J., Rothberg, B. S., Madesh, M. & Gill, D. L. 2012. STIM proteins: dynamic calcium signal transducers. *Nat Rev Mol Cell Biol,* 13**,** 549-65.

Soboloff, J., Spassova, M. A., Hewavitharana, T., He, L. P., Xu, W., Johnstone, L. S., Dziadek, M. A. & Gill, D. L. 2006a. STIM2 is an inhibitor of STIM1-mediated store-operated Ca2+ Entry. *Curr Biol,* 16**,** 1465-70.

Soboloff, J., Spassova, M. A., Tang, X. D., Hewavitharana, T., Xu, W. & Gill, D. L. 2006b. Orai1 and STIM reconstitute store-operated calcium channel function. *J Biol Chem,* 281**,** 20661-5.

Srikanth, S., Jew, M., Kim, K. D., Yee, M. K., Abramson, J. & Gwack, Y. 2012. Junctate is a Ca2+-sensing structural component of Orai1 and stromal interaction molecule 1 (STIM1). *Proc Natl Acad Sci U S A,* 109**,** 8682-7.

Srikanth, S., Jung, H. J., Kim, K. D., Souda, P., Whitelegge, J. & Gwack, Y. 2010. A novel EF-hand protein, CRACR2A, is a cytosolic Ca2+ sensor that stabilizes CRAC channels in T cells. *Nat Cell Biol,* 12**,** 436-46.

Stathopulos, P. B., Li, G. Y., Plevin, M. J., Ames, J. B. & Ikura, M. 2006. Stored Ca2+ depletion-induced oligomerization of stromal interaction molecule 1 (STIM1) via the EF-SAM region: An initiation mechanism for capacitive Ca2+ entry. *J Biol Chem,* 281**,** 35855-62.

Stathopulos, P. B., Schindl, R., Fahrner, M., Zheng, L., Gasmi-Seabrook, G. M., Muik, M., Romanin, C. & Ikura, M. 2013. STIM1/Orai1 coiled-coil interplay in the regulation of store-operated calcium entry. *Nat Commun,* 4**,** 2963.

Stathopulos, P. B., Zheng, L. & Ikura, M. 2009. Stromal interaction molecule (STIM) 1 and STIM2 calcium sensing regions exhibit distinct unfolding and oligomerization kinetics. *J Biol Chem,* 284**,** 728-32.

Stathopulos, P. B., Zheng, L., Li, G. Y., Plevin, M. J. & Ikura, M. 2008. Structural and mechanistic insights into STIM1-mediated initiation of store-operated calcium entry. *Cell,* 135**,** 110-22.

Stiber, J., Hawkins, A., Zhang, Z. S., Wang, S., Burch, J., Graham, V., Ward, C. C., Seth, M., Finch, E., Malouf, N., Williams, R. S., Eu, J. P. & Rosenberg, P. 2008. STIM1 signalling controls store-operated calcium entry required for development and contractile function in skeletal muscle. *Nat Cell Biol,* 10**,** 688-97.

Subedi, K. P., Ong, H. L., Son, G. Y., Liu, X. & Ambudkar, I. S. 2018. STIM2 Induces Activated Conformation of STIM1 to Control Orai1 Function in ER-PM Junctions. *Cell Rep,* 23**,** 522-534.

Takemura, H. & Putney, J. W., Jr. 1989. Capacitative calcium entry in parotid acinar cells. *Biochem J,* 258**,** 409-12.

Tao, S., Yamazaki, D., Komazaki, S., Zhao, C., Iida, T., Kakizawa, S., Imaizumi, Y. & Takeshima, H. 2013. Facilitated hyperpolarization signaling in vascular smooth muscle-overexpressing TRIC-A channels. *J Biol Chem,* 288**,** 15581-9.

Thompson, J. L. & Shuttleworth, T. J. 2013. Molecular basis of activation of the arachidonate-regulated Ca2+ (ARC) channel, a store-independent Orai channel, by plasma membrane STIM1. *J Physiol,* 591**,** 3507-23.

Tiapko, O., Shrestha, N., Lindinger, S., Guedes De La Cruz, G., Graziani, A., Klec, C., Butorac, C., Graier, W. F., Kubista, H., Freichel, M., Birnbaumer, L., Romanin, C., Glasnov, T. & Groschner, K. 2019. Lipid-independent control of endothelial and neuronal TRPC3 channels by light. *Chem Sci,* 10**,** 2837-2842.

Uehara, A., Yasukochi, M., Imanaga, I., Nishi, M. & Takeshima, H. 2002. Store-operated Ca2+ entry uncoupled with ryanodine receptor and junctional membrane complex in heart muscle cells. *Cell Calcium,* 31**,** 89-96.

Vaeth, M. & Feske, S. 2018. Ion channelopathies of the immune system. *Curr Opin Immunol,* 52**,** 39-50.

Venturi, E., Matyjaszkiewicz, A., Pitt, S. J., Tsaneva-Atanasova, K., Nishi, M., Yamazaki, D., Takeshima, H. & Sitsapesan, R. 2013. TRIC-B channels display labile gating: evidence from the TRIC-A knockout mouse model. *Pflugers Arch,* 465**,** 1135-48.

Vig, M., Beck, A., Billingsley, J. M., Lis, A., Parvez, S., Peinelt, C., Koomoa, D. L., Soboloff, J., Gill, D. L., Fleig, A., Kinet, J. P. & Penner, R. 2006a. CRACM1 multimers form the ion-selective pore of the CRAC channel. *Curr Biol,* 16**,** 2073-9.

Vig, M., Peinelt, C., Beck, A., Koomoa, D. L., Rabah, D., Koblan-Huberson, M., Kraft, S., Turner, H., Fleig, A., Penner, R. & Kinet, J. P. 2006b. CRACM1 is a plasma membrane protein essential for store-operated Ca2+ entry. *Science,* 312**,** 1220-3.

Voelkers, M., Salz, M., Herzog, N., Frank, D., Dolatabadi, N., Frey, N., Gude, N., Friedrich, O., Koch, W. J., Katus, H. A., Sussman, M. A. & Most, P. 2010. Orai1 and Stim1 regulate normal and hypertrophic growth in cardiomyocytes. *J Mol Cell Cardiol,* 48**,** 1329-34.

Walsh, C. M., Chvanov, M., Haynes, L. P., Petersen, O. H., Tepikin, A. V. & Burgoyne, R. D. 2009. Role of phosphoinositides in STIM1 dynamics and store-operated calcium entry. *Biochem J,* 425**,** 159-68.

Walsh, C. M., Doherty, M. K., Tepikin, A. V. & Burgoyne, R. D. 2010. Evidence for an interaction between Golli and STIM1 in store-operated calcium entry. *Biochem J,* 430**,** 453-60.

Wang, X. H., Su, M., Gao, F., Xie, W., Zeng, Y., Li, D. L., Liu, X. L., Zhao, H., Qin, L., Li, F., Liu, Q., Clarke, O. B., Lam, S. M., Shui, G. H., Hendrickson, W. A. & Chen, Y. H. 2019. Structural basis for activity of TRIC counter-ion channels in calcium release. *Proc Natl Acad Sci U S A*.

Wang, Y., Deng, X., Mancarella, S., Hendron, E., Eguchi, S., Soboloff, J., Tang, X. D. & Gill, D. L. 2010. The calcium store sensor, STIM1, reciprocally controls Orai and CaV1.2 channels. *Science,* 330**,** 105-9.

Wedel, B., Boyles, R. R., Putney, J. W., Jr. & Bird, G. S. 2007. Role of the store-operated calcium entry proteins Stim1 and Orai1 in muscarinic cholinergic receptor-stimulated calcium oscillations in human embryonic kidney cells. *J Physiol,* 579**,** 679-89.

Wei-Lapierre, L., Carrell, E. M., Boncompagni, S., Protasi, F. & Dirksen, R. T. 2013. Orai1-dependent calcium entry promotes skeletal muscle growth and limits fatigue. *Nat Commun,* 4**,** 2805.

Williams, R. T., Manji, S. S., Parker, N. J., Hancock, M. S., Van Stekelenburg, L., Eid, J. P., Senior, P. V., Kazenwadel, J. S., Shandala, T., Saint, R., Smith, P. J. & Dziadek, M. A. 2001. Identification and characterization of the STIM (stromal interaction molecule) gene family: coding for a novel class of transmembrane proteins. *Biochem J,* 357**,** 673-85.

Willoughby, D., Everett, K. L., Halls, M. L., Pacheco, J., Skroblin, P., Vaca, L., Klussmann, E. & Cooper, D. M. 2012. Direct binding between Orai1 and AC8 mediates dynamic interplay between Ca2+ and cAMP signaling. *Sci Signal,* 5**,** ra29.

Wu, M. M., Buchanan, J., Luik, R. M. & Lewis, R. S. 2006. Ca2+ store depletion causes STIM1 to accumulate in ER regions closely associated with the plasma membrane. *J Cell Biol,* 174**,** 803-13.

Yamashita, M., Yeung, P. S., Ing, C. E., Mcnally, B. A., Pomes, R. & Prakriya, M. 2017. STIM1 activates CRAC channels through rotation of the pore helix to open a hydrophobic gate. *Nat Commun,* 8**,** 14512.

Yamazaki, D., Komazaki, S., Nakanishi, H., Mishima, A., Nishi, M., Yazawa, M., Yamazaki, T., Taguchi, R. & Takeshima, H. 2009. Essential role of the TRIC-B channel in Ca2+ handling of alveolar epithelial cells and in perinatal lung maturation. *Development,* 136**,** 2355-61.

Yamazaki, D., Tabara, Y., Kita, S., Hanada, H., Komazaki, S., Naitou, D., Mishima, A., Nishi, M., Yamamura, H., Yamamoto, S., Kakizawa, S., Miyachi, H., Yamamoto, S., Miyata, T., Kawano, Y., Kamide, K., Ogihara, T., Hata, A., Umemura, S., Soma, M., Takahashi, N., Imaizumi, Y., Miki, T., Iwamoto, T. & Takeshima, H. 2011. TRIC-A channels in vascular smooth muscle contribute to blood pressure maintenance. *Cell Metab,* 14**,** 231-41.

Yang, H., Hu, M., Guo, J., Ou, X., Cai, T. & Liu, Z. 2016. Pore architecture of TRIC channels and insights into their gating mechanism. *Nature,* 538**,** 537-541.

Yang, X., Jin, H., Cai, X., Li, S. & Shen, Y. 2012. Structural and mechanistic insights into the activation of Stromal interaction molecule 1 (STIM1). *Proc Natl Acad Sci U S A,* 109**,** 5657-62.

Yazawa, M., Ferrante, C., Feng, J., Mio, K., Ogura, T., Zhang, M., Lin, P. H., Pan, Z., Komazaki, S., Kato, K., Nishi, M., Zhao, X., Weisleder, N., Sato, C., Ma, J. & Takeshima, H. 2007. TRIC channels are essential for Ca2+ handling in intracellular stores. *Nature,* 448**,** 78-82.

Yen, M., Lokteva, L. A. & Lewis, R. S. 2016. Functional Analysis of Orai1 Concatemers Supports a Hexameric Stoichiometry for the CRAC Channel. *Biophys J,* 111**,** 1897-1907.

Yu, F., Sun, L., Hubrack, S., Selvaraj, S. & Machaca, K. 2013. Intramolecular shielding maintains the ER Ca(2)(+) sensor STIM1 in an inactive conformation. *J Cell Sci,* 126**,** 2401-10.

Yuan, J. P., Zeng, W., Dorwart, M. R., Choi, Y. J., Worley, P. F. & Muallem, S. 2009. SOAR and the polybasic STIM1 domains gate and regulate Orai channels. *Nat Cell Biol,* 11**,** 337-43.

Yuan, J. P., Zeng, W., Huang, G. N., Worley, P. F. & Muallem, S. 2007. STIM1 heteromultimerizes TRPC channels to determine their function as store-operated channels. *Nat Cell Biol,* 9**,** 636-45.

Zeng, W., Yuan, J. P., Kim, M. S., Choi, Y. J., Huang, G. N., Worley, P. F. & Muallem, S. 2008. STIM1 gates TRPC channels, but not Orai1, by electrostatic interaction. *Mol Cell,* 32**,** 439-48.

Zhang, H., Sun, A. Y., Kim, J. J., Graham, V., Finch, E. A., Nepliouev, I., Zhao, G., Li, T., Lederer, W. J., Stiber, J. A., Pitt, G. S., Bursac, N. & Rosenberg, P. B. 2015. STIM1-Ca2+ signaling modulates automaticity of the mouse sinoatrial node. *Proc Natl Acad Sci U S A,* 112**,** E5618-27.

Zhang, S. L., Yeromin, A. V., Zhang, X. H., Yu, Y., Safrina, O., Penna, A., Roos, J., Stauderman, K. A. & Cahalan, M. D. 2006. Genome-wide RNAi screen of Ca(2+) influx identifies genes that regulate Ca(2+) release-activated Ca(2+) channel activity. *Proc Natl Acad Sci U S A,* 103**,** 9357-62.

Zhang, S. L., Yu, Y., Roos, J., Kozak, J. A., Deerinck, T. J., Ellisman, M. H., Stauderman, K. A. & Cahalan, M. D. 2005. STIM1 is a Ca2+ sensor that activates CRAC channels and migrates from the Ca2+ store to the plasma membrane. *Nature,* 437**,** 902-5.

Zhao, G., Li, T., Brochet, D. X., Rosenberg, P. B. & Lederer, W. J. 2015. STIM1 enhances SR Ca2+ content through binding phospholamban in rat ventricular myocytes. *Proc Natl Acad Sci U S A,* 112**,** E4792-801.

Zhao, X., Yamazaki, D., Park, K. H., Komazaki, S., Tjondrokoesoemo, A., Nishi, M., Lin, P., Hirata, Y., Brotto, M., Takeshima, H. & Ma, J. 2010. Ca2+ overload and sarcoplasmic reticulum instability in tric-a null skeletal muscle. *J Biol Chem,* 285**,** 37370-6.

Zheng, H., Zhou, M. H., Hu, C., Kuo, E., Peng, X., Hu, J., Kuo, L. & Zhang, S. L. 2013. Differential roles of the C and N termini of Orai1 protein in interacting with stromal interaction molecule 1 (STIM1) for Ca2+ release-activated Ca2+ (CRAC) channel activation. *J Biol Chem,* 288**,** 11263-72.

Zheng, L., Stathopulos, P. B., Schindl, R., Li, G. Y., Romanin, C. & Ikura, M. 2011. Auto-inhibitory role of the EF-SAM domain of STIM proteins in store-operated calcium entry. *Proc Natl Acad Sci U S A,* 108**,** 1337-42.

Zhou, Y., Cai, X., Loktionova, N. A., Wang, X., Nwokonko, R. M., Wang, X., Wang, Y., Rothberg, B. S., Trebak, M. & Gill, D. L. 2016. The STIM1-binding site nexus remotely controls Orai1 channel gating. *Nat Commun,* 7**,** 13725.

Zhou, Y., Mancarella, S., Wang, Y., Yue, C., Ritchie, M., Gill, D. L. & Soboloff, J. 2009. The short N-terminal domains of STIM1 and STIM2 control the activation kinetics of Orai1 channels. *J Biol Chem,* 284**,** 19164-8.

Zhou, Y., Meraner, P., Kwon, H. T., Machnes, D., Oh-Hora, M., Zimmer, J., Huang, Y., Stura, A., Rao, A. & Hogan, P. G. 2010a. STIM1 gates the store-operated calcium channel ORAI1 in vitro. *Nat Struct Mol Biol,* 17**,** 112-6.

Zhou, Y., Nwokonko, R. M., Cai, X., Loktionova, N. A., Abdulqadir, R., Xin, P., Niemeyer, B. A., Wang, Y., Trebak, M. & Gill, D. L. 2018. Cross-linking of Orai1 channels by STIM proteins. *Proc Natl Acad Sci U S A,* 115**,** E3398-E3407.

Zhou, Y., Ramachandran, S., Oh-Hora, M., Rao, A. & Hogan, P. G. 2010b. Pore architecture of the ORAI1 store-operated calcium channel. *Proc Natl Acad Sci U S A,* 107**,** 4896-901.

Zhou, Y., Srinivasan, P., Razavi, S., Seymour, S., Meraner, P., Gudlur, A., Stathopulos, P. B., Ikura, M., Rao, A. & Hogan, P. G. 2013. Initial activation of STIM1, the regulator of store-operated calcium entry. *Nat Struct Mol Biol,* 20**,** 973-81.

Zitt, C., Strauss, B., Schwarz, E. C., Spaeth, N., Rast, G., Hatzelmann, A. & Hoth, M. 2004. Potent inhibition of Ca2+ release-activated Ca2+ channels and T-lymphocyte activation by the pyrazole derivative BTP2. *J Biol Chem,* 279**,** 12427-37.

Zsolnay, V., Fill, M. & Gillespie, D. 2018. Sarcoplasmic Reticulum Ca(2+) Release Uses a Cascading Network of Intra-SR and Channel Countercurrents. *Biophys J,* 114**,** 462-473.

Zweifach, A. & Lewis, R. S. 1993. Mitogen-regulated Ca2+ current of T lymphocytes is activated by depletion of intracellular Ca2+ stores. *Proc Natl Acad Sci U S A,* 90**,** 6295-9.

Zweifach, A. & Lewis, R. S. 1995. Rapid inactivation of depletion-activated calcium current (ICRAC) due to local calcium feedback. *J Gen Physiol,* 105**,** 209-26.

6. Appendix

6.1 List of publications during the Ph.D. dissertation

1. Tiapko O*, **Shrestha N***, Lindinger S, Guedes de la Cruz G, Klec C, Butorac C, Graier WF Kubista H, Freichel M, Birnbaumer L, Romanin C, Glasnov T, Groschner K. 2018. Lipid-independent control of endothelial and neuronal TRPC3 channels by light. Chem Sci, 10(9), 2837-2842. *shared first authors (contributed equally)
2. Groschner K, **Shrestha N**, Fameli N. 2018. Non-Orai Partners of STIM Proteins: Role in ER-PM Communication and Ca^{2+} Signaling. In: Kozak JA, Putney JW, Jr., editors. Calcium Entry Channels in Non-Excitable Cells. Boca Raton (FL), p. 177-197.
3. Koyani CN, Trummer C, **Shrestha N**, Scheruebel S, Bourgeois B, Plastira I, Kickmaier S, Sourij H, Rainer PP, Madl T, Sattler W, Pelzmann B, Malle E and von Lewinski D. 2018. Saxagliptin but Not Sitagliptin Inhibits CaMKII and PKC via DPP9 Inhibition in Cardiomyocytes. Front Physiol, 9, 1622.
4. Lichtenegger M, Tiapko O, Svobodova B, Stockner T, Glasnov TN, Schreibmayer W, Platzer D, de la Cruz GG, Krenn S, Schober R, **Shrestha N**, Schindl R, Romanin C, Groschner K. 2018. An optically controlled probe identifies lipid-gating fenestrations within the TRPC3 channel. Nat Chem Biol, 14(4), 396-404.
5. Koyani CN, Kolesnik E, Wolkart G, **Shrestha N**, Scheruebel S, Trummer C, Zorn-Pauly K, Hammer A, Lang P, Reicher H, Maechler H, Groschner K, Mayer B, Rainer PP, Sourij H, Sattler W, Malle E, Pelzmann B, von Lewinski D. 2017. Dipeptidyl peptidase-4 independent cardiac dysfunction links saxagliptin to heart failure. Biochem Pharmacol, 145, 64-80.
6. Di Giuro CML, **Shrestha N**, Malli R, Groschner K, van Breemen C, Fameli N. 2017. Na^{+}/Ca^{2+} exchangers and Orai channels jointly refill endoplasmic reticulum (ER) Ca^{2+} via ER nanojunctions in vascular endothelial cells. Pflugers Arch, 469(10), 1287-1299.
7. Groschner K, **Shrestha N**, Fameli N. 2017. Cardiovascular and Hemostatic Disorders: SOCE in Cardiovascular Cells-Emerging Targets for Therapeutic Intervention. Adv Exp Med Biol, 993, 473-503.
8. Chauvet S, Jarvis L, Chevallet M, **Shrestha N**, Groschner K, Bouron A. 2016. Pharmacological Characterization of the Native Store-Operated Calcium Channels of Cortical Neurons from Embryonic Mouse Brain. Front Pharmacol, 7, 486.